University of South-Eastern Norway
Faculty of Technology, Natural Sciences and Maritime Studies

Doctoral dissertation no. 54
2019

Sindre Søpstad

Flexible electrochemical sensor platform

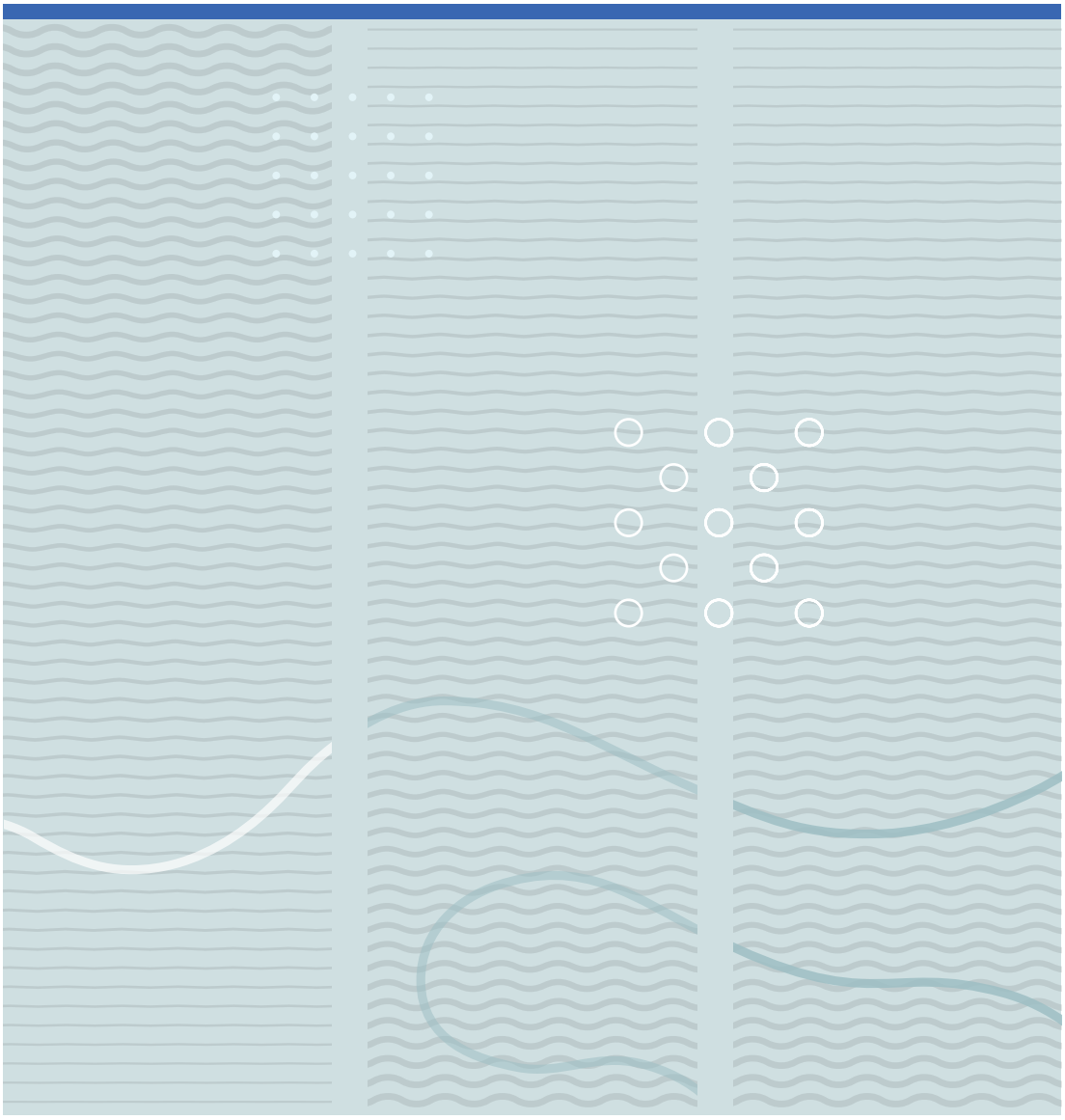

Sindre Søpstad

Flexible electrochemical sensor platform

A PhD dissertation in
Applied Micro- and Nanosystems

Faculty of Technology, Natural Sciences and Maritime Studies
University of South-Eastern Norway
Horten, 2019

Doctoral dissertations at the University of South-Eastern Norway no. 54

ISSN: 2535-5244(print)
ISSN: 2535-5252 (online)

ISBN: 978-82-7860-404-5(print)
ISBN: 978-82-7860-405-2 (online)

Print: University of South-Eastern Norway

Preface

This doctoral thesis is submitted for the degree of Doctor of Philosophy at the Faculty of Technology and Maritime Science, University of South-Eastern Norway (USN), Norway. The work was carried out between August 2015 and December 2018 at the Department of Microsystems (USN) under the supervision of Associate Professor Kristin Imenes and Professor Erik Andrew Johannessen.

This work is financially supported by the Norwegian Ministry of Education and Research (KD) program at University of South-Eastern Norway, and the Norwegian Ph. D. Network on Nanotechnology for Microsystems (221860/F40).

Abstract

Bringing an electroanalytical assay from the laboratory to the level of a commercially or clinically viable product often requires substantial cost, effort and time. While the real value may lie in the assay and sensor development, it has to be bundled with instrumentation, packaging, and readout software in order to function as a single, handleable unit. To unburden the sensor developer by not having to design the architecture to support the sensor, a universal electrochemical sensor platform, the ecFlex, has been developed. It is made small (25 mm × 29 mm, 1.2 g) by limiting the number of electronic components, and portable through data transfer via Bluetooth Low Energy to either PC or smartphone, and battery operation. Universality was realized by implementing several electrochemical measurement techniques such as chronoamperometry, squarewave voltammetry and open-circuit potentiometry. The platform allows for different material selections for the integrated screen-printed electrodes, as well as the option of interfacing external electrodes. Applicability was secured using a flexible printed circuit as the substrate to allow conformity towards different applications, including wearable sensors. The voltammetric range was limited to ±720 with 60 mV increments and ±872 µA with 0.87 nA resolution, whereas potentiometric capabilities had a useable range of 10-300 mV with 310 µV resolution. Whereas the power consumption depends upon the electrochemical technique used, cell current passed and transmission intervals for telemetry, the sensor platform was able to run continuously for 14h under the conditions of open-circuit potentiometric mode with, and 0.5 s transmission intervals on a 25 mAh battery.

The performance of one of the key components of electrochemical sensor applications, the reference electrode, was investigated in detail. Specifically, the long-term stability of five different screen-printed material systems in a phosphate buffer was characterized by the means of an automated open circuit potentiometric measurement setup. Among screen-printed Pt, Ag/Pd, Ag, and Ag/AgCl of atomic ratios 3:1 and 9:1,

only 3:1 Ag/AgCl remained stable throughout 40 days of continuous operation, as determined by the deviation from their initial potential. Its stability was attributed to having a strong potential-determining reaction with the dissolved Cl in the solution, and having sufficient AgCl preventing full dissolution during the course of the experiment. As a tradeoff, the dissolved AgCl caused a local build-up of Cl^- that yielded a higher drift (-0.2 mV day^{-1}) than the 9:1 Ag/AgCl electrodes (-0.1 mV day^{-1}). Thus, the 3:1 Ag/AgCl ink was selected as the reference electrode for the present sensor applications, and in one case also for the working and counter electrodes.

The role of the reference electrode was further studied through finite element analysis. The particular case for space-saving applications using a combined reference and counter electrode, and a similarly sized working electrode was investigated. It was found that the polarization of the reference electrode could shift the working electrode potential so close to the reversible potential of the working electrode reaction that it severely affected its sensitivity and drift, compared to using a three-electrode system. More specifically, the high current density through the reference electrode caused a high enough deficiency of Cl^- compared to the bulk solution that its potential, and correspondingly the potential of the working electrode, shifted positively. The working electrode was shifted so close to the redox potential of the electrode reaction that it kinetically limited the electrode, as well as adding contributions of the reverse reaction, resulting in a lowering of the analytical sensitivity. The continuous depletion of Cl^- additionally caused a drift in the electrode potentials, and consequently the cell current. The effect was verified through experiment. One of the implications is that there may be sensor systems in the real world suffering a performance loss due to an insufficiently dimensioned counter/reference electrode. The simulated sensor response gave up to 14 % deviation from the ideal analytical signal.

The sensor platform was demonstrated for analytical applications through the determination of capsaicinoid content in chili-derived products, and pH and Cl^- quantification. A simplified measurement technique, coarsely-stepped cyclic squarewave voltammetry, was developed, demonstrating that more refined techniques

that require more precise, and thus expensive equipment, such as cyclic voltammetry, might be redundant for certain applications. A rinsing protocol was developed that made the screen-printed carbon working electrode reusable for at least 20 measurements.

Potentiometric sensors for measuring pH in the range 2-9 (± 0.43) with half-nernstian sensitivity (26 mV) was designed based on carbon electrodes containing a redox couple coated with graphene oxide. A solid-state reference electrolyte was employed to allow sample matrices of unknown Cl^- content. Moreover, a reagentless Cl^- sensor was made. The sensor was based around the technique of squarewave amperometry on a three-electrode system where all electrodes were identical Cl^- selective Ag/AgCl electrodes. The platform was able detect Cl^- in the range pCl 3 to 0 (± 0.27).

Overall, the work demonstrates a universal and portable platform compatible with different electrochemical detection principles and the determination of several analytes that are important to a range of applications, at a low material cost. The open platform allows research and commercial efforts to quickly transform from a proof-of-concept, to something more like a product, reducing both the cost and effort required for prototype design.

Keywords: Electrochemical sensors, biosensors, flexible electronics, open-source electrochemical instruments

Abbreviations

ADC Analog-to-digital converter
BLE Bluetooth Low Energy
CA Chronoamperometry
CV Cyclic voltammetry
DC Direct current
DPV Differential pulse voltammetry
EIS Electrochemical impedance spectroscopy
FDM Finite difference method
FEA Finite element analysis
FPC Flexible printed circuit
GUI Graphical user interface
IOT Internet-of-things
ISE Ion selective electrode
LOD Limit of detection
MA Multistep amperometry
OCP Open-circuit potential
PBS Phosphate buffered saline
PCB Printed circuit board
PSoC Programmable system-on-chip
RDS Rate determining step
RE Reference electrode
SWA Squarewave amperometry
SWV Squarewave voltammetry
WE Working electrode

List of contributions

Peer-reviewed journal papers included in the thesis

Articles omitted from online version due to publisher's restrictions

Article 1

S. Søpstad, E. A. Johannessen, F. Seland, and K. Imenes (2018). Long-term stability of screen-printed pseudo-reference electrodes for electrochemical biosensors, *Electrochim. Acta*, vol. 287, pp. 29–36. doi: 10.1016/j.electacta.2018.08.045

Article 2

S. Søpstad, K. Imenes, and E. A. Johannessen (2019). Hybrid electrochemical sensor platform for capsaicin determination using coarsely stepped cyclic squarewave voltammetry, *Biosens. Bioelectron.*, vol. 130, pp. 374–381. doi: 10.1016/j.bios.2018.09.036

Article 3

S. Søpstad, K. Imenes, and E. A. Johannessen (2019). Chloride and pH detection on flexible a electrochemical sensor platform, *IEEE Sensors Journal (Early Access),* doi: 10.1109/JSEN.2019.2944407

Article 4

S. Søpstad, K. Imenes, and E. A. Johannessen (2019). Analytical errors in biosensors employing combined counter/reference electrodes. Submitted to *Results in Chemistry* July 2019

Peer-reviewed journal papers not included in the thesis

Article 5

S. Damiati, M. Peacock, R. Mhanna, S. Søpstad, U. B. Sleytr, and B. Schuster (2018), Bioinspired detection sensor based on functional nanostructures of S-proteins to target the folate receptors in breast cancer cells, *Sensors Actuators B Chem.*, vol. 267, pp. 224–230

Article 6

C. Day, S. Søpstad, H. Ma, C. Jiang, A. Nathan, S.R. Elliott, F.E. Karet Frankl, T. Hutter (2018), Impedance-based sensor for potassium ions, *Anal. Chim. Acta*, vol. 1034, pp. 39–45. doi: 10.1016/j.aca.2018.06.044

Article 7

S. Damiati, C. Haslam, S. Sopstad, M. Peacock, T. Whitley, P. Davey, S.A. Awan, Sensitivity Comparison of Macro- and Micro-Electrochemical Biosensors for Human Chorionic Gonadotropin (hCG) Biomarker Detection, IEEE Access. (2019) 1–1. doi: 10.1109/ACCESS.2019.2928132.

Peer-reviewed conference contributions

Article 8

S. Søpstad, K. Imenes, and E. A. Johannessen (2018). Hybrid electrochemical sensor platform – Determination of capsaicin. Presented at the 28th anniversary world Biosensors Congress (2018, Miami).

Table of contents

1 Background and motivation

This work was initiated by the increased demand for generic platforms capable of performing electrochemical assays in more affordable, portable and simple ways than what is currently available. There is considerable cost and effort associated with bringing a laboratory conceived assay to the level of a commercially or clinically valid product [1]. The effort increases for countries with limited technological infrastructure and resources, and where the need for the technology might also be the greatest [2]. This is a contribution to help bridge the gap between the high-threshold lab-to-field technology transfer in the area of electrochemical biosensors, that being commercial distribution, clinical testing or simply proving that the assay works outside the walls of the lab.

Thus, the main focus of this project has been to:

> Develop and manufacture a miniature electrochemical biosensor platform, where transducer, instrumentation and wireless power transfer is integrated, with emphasis on manufacturability, versatility and ease-of-use.

The primary objective was realized through the implementation and resolution of the following four secondary objectives:

1. Design, manufacture and programming of said platform
2. In-depth investigation of at least one of the platform's key sub-components
3. Demonstrate its use for several analytes
4. Expand its applicability by implementing several instrumental modes

1.1 Multidisciplinarity

The work involves aspects from many scientific fields. Perhaps most strongly is electronics, microfabrication, electrochemistry and biosensor technology. It may best be summarized by the overall term *applied microsystems*. Applied microsystems, as interpreted by the author, bridge many fundamental sciences with the common cause of producing a compact, integrated sensor or actuator system as solutions for real world problems.

1.2 Sensors in society

The past decade has been the birthing years of the complete interconnectedness of electronics and information. The ability to mass distribute sensor systems and collecting Big Data is rapidly changing the way humans perceive and interpret our home planet and its surrounding space. This has been made possible by the convergence of several technological innovations such as microcontrollers with reduced power consumption offering a high degree of integration combined with an increase in energy density of energy storage of portable power supplies like batteries and supercapacitors. Renewable energy and self-powered devices [3], miniaturization, smart packaging and our ever-expanding reach of wireless transfer of information have culminated in the popular term the Internet of Things (IOT), where humans can effortlessly communicate with countless machines that may aid in every imaginable task. Sensors play an integral role as they are responsible for providing the information that makes the foundation for decision making. Hence, the accuracy of this source of information is paramount in order to ensure a correct response by humans or actuators involved in the decision making process.

One good example of sensor networks used today is in atmospheric meteorology, where these are distributed around the globe in order to read and help predict the weather [4]. Outside our planet, robots equipped with numerous sensors and actuators are helping us to increase our knowledge of neighboring planets [5], as well as remote galaxies. Hospitals and medical patients, even animals [6], rely on the information of

instruments monitoring important markers for disease. Closed-loop systems are becoming more common, where the sensor provides feedback to the actuator for auto-administering of drugs. One example is continuous blood glucose sensors that are coupled with an insulin pump to help diabetics regulate their glucose level [7], [8]. The military records information on individual troop members through wearable sensors and drones [9]. Sensors are also becoming an increasingly important part of professional athleticism, where parameters such as O_2, glucose and lactate in bodily fluids can be used to optimize training regimes and further improve athletic performance [10]. One often looks to the mature automobile industry where sensors are now a well-integrated part of the machinery, numbering over a hundred sensors for some vehicles [11], [12]. We depend heavily upon mobile phones, which are packed with sensors, but also as a source of interpreting and visualizing sensory input. In addition, pharmaceutical production, food and beverage industry, personal safety, environmental monitoring, screening of material integrity in constructions [13]–[16], are only a few examples of how sensors and actuators are becoming an integrated part of society.

1.3 Electrochemical transducers

The transducer is the device responsible for translating the analytical signal from one energy domain to another. This signal, whether it is electromechanical, electrooptical, electrochemical, electromagnetic, thermoelectric or any hybrid combination of these, may be processed and visualized to yield important information about the corresponding non-electrical domain.

In analytical chemistry, electrochemical transducers are in general used for chemical analysis. A schematic representation of the general sensing principle involving electrochemical transducers is shown in Figure 1.1. The quantity and match of the chemical species of interest is the original signal. This is converted to electrical energy by either charge transfer by way of electrons or accumulation of the charged species at the interface. The analyte of interest is discriminated from other species by the help of a recognition element [17]–[19]. The transducers are attractive due to their often simple

construction, consisting of two or more metal or semiconductor electrodes, and electrical tracks passivated by an insulator, on some form of mechanical support. Their inherent simplicity leaves a potential for miniaturization, and makes them suitable for mass production, which further means cost effectiveness and the ability for mass distribution, yielding sensors available to the general public. Electrochemical sensors are known to be able to rapidly measure the analyte levels with high precision, affinity, accuracy and reliability, even in the hands of unskilled operators [20]. One of the limiting processes for a sensor to achieve all these perks is the massive effort associated with transferring the assay from a laboratory environment into an accessible product.

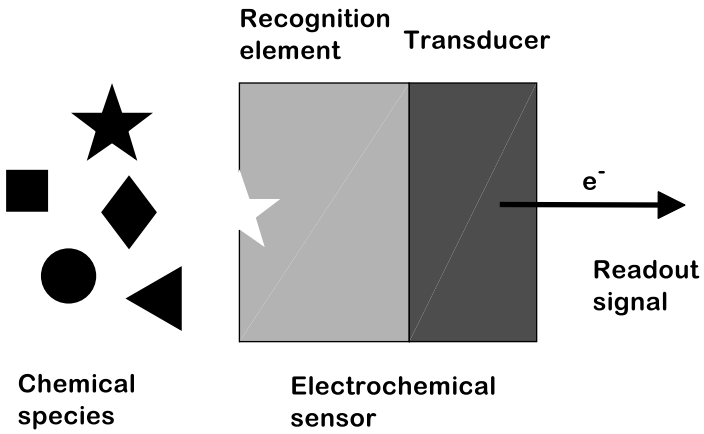

Figure 1.1. Schematic representation of an electrochemical sensor and its governing operating principle. The geometric shapes represent chemical species, where only one is a good match for the recognition element. The recognized species is converted to an electrical signal by the transducer.

The graph in Figure 1.2 exemplifies the growing interest in electrochemical biosensors from the increase in annual academic publications on the topic. In the year 2017, electrochemical biosensors were responsible for 25 % of the publications related to biosensors. A note of caution is appropriate when interpreting the number of publications on a topic as a direct metric for scientific interest. Throughout these four decades the number of publications has increasingly become a metric for academic success, and there is growing concern that publication pressure leads to less accurate and significant reports [21], [22]. Even so, progressing from 0 to over 1000 yearly

publications is inarguably a result of growing interest, even if the impact of the numbers is debatable.

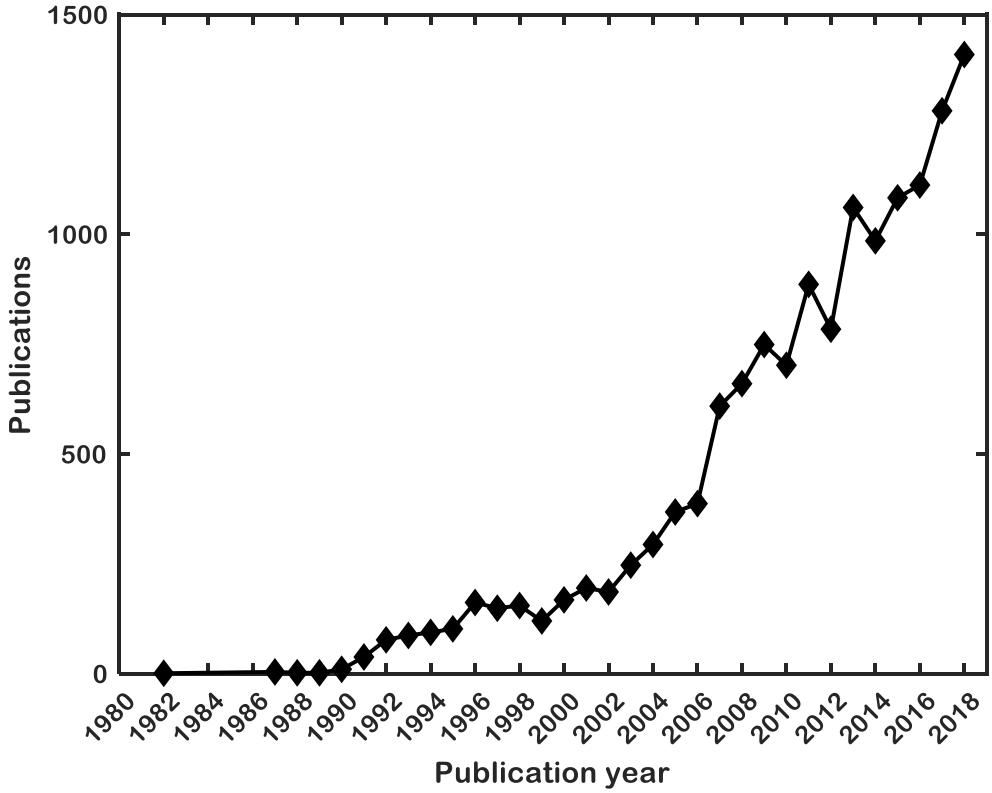

Figure 1.2. Yearly publications based on the keyword "biosensor" filtered by the topic of "electrochemistry". Data extracted from "Web of Knowledge" 15th Jun 2019.*

1.4 Screen-printing

The commercial success of electrochemical sensors is often credited to the 1990s success story of sensors systems for point-of-care (POC) monitoring of blood glucose in people suffering from diabetes mellitus. The system consists of disposable electrochemical test strips for blood analysis, and a hand-held unit for sample readout. Although the startup cost and associated research was considerable, sensors and insulin pumps are currently (2018) responsible for a yearly market share of $21.7B, with a projected outlook of $32.9B, by the year 2025 [23], [24]. Clearly, if we could have more success stories like this, electrochemical sensors and sensor systems would benefit people even more.

A big part of this success story was made possible through implementation of screen-printing as a microfabrication method. Screen-printing enables the patterning of substrates by pushing a viscous paste (3-10 Pa s) through openings in a stencil or screen by a squeegee blade, as demonstrated in Figure 1.3. The components of the paste is the active material, such as carbon or gold particles, solvents to suspend and disperse these particles, and agents for tailoring printability, adhesion and cohesion. The paste is thixotropically engineered such that when pressurized by the laterally moving, angled squeegee, it undergoes sheer thinning, allowing it to flow through the openings, and immediately thickens once the pressure is relieved. The thickness of the print is decided by the thickness of the screen and/or the gap between screen and substrate. The print is then cured, typically around 100 °C, mainly to accelerate the evaporation of solvents, leaving behind the desired, patterned material. Elevated temperatures (700 – 900 °C) may also be used to make continuous solids, rather than physically interconnected particles. The printing and curing cycles are additive, such that any number of complex structures and materials may be printed. Metters et al. [25] gives an excellent review of screen-printing for electrochemical biosensors, whereas an extensive practical guide is provided by Alan Hobby [26].

The technique originates from making decorative prints on textiles, like t-shirts, and has reputed history 2000 years ago in China [26]. The first recorded history of screen-printing on textiles was in 1850 in England and France. It has since been adapted by the electronics industry for patterning of electronic circuits and solder paste [26]. It is frequently used in hybrid electronics for high-temperature applications, although biosensors make up a significant portion of the market [27]. Automated screen-printing can mass-produce electrochemical sensors with a high degree of reproducibility. Another strength of screen-printing is its ever-growing material portfolio [28]. Just about any material can be suspended in a paste consisting of a multitude of solvents and binders and printed onto nearly any kind of surface [29]. Furthermore, screen-printing can be used to pattern the active chemistry, including enzymes or antibodies onto, or even as part for the electrode ink [29]–[32], meaning no further processing is

necessary. The clear disadvantage of screen-printing is the cruder line-definition, often limited to 100 µm, compared to silicon microfabrication, which makes it unsuitable for highly integrated electronics. Additionally, the current state of the art in screen-printing prohibits the utilization of microelectrodes. Microelectrodes are known to benefit from higher current density due to radial diffusion patterns, low non-faradaic current contribution and reduced ohmic drop [33]. Advances are being made to facilitate microelectrodes through screen-printing, but has yet to see any wide-spread application [34], [35].

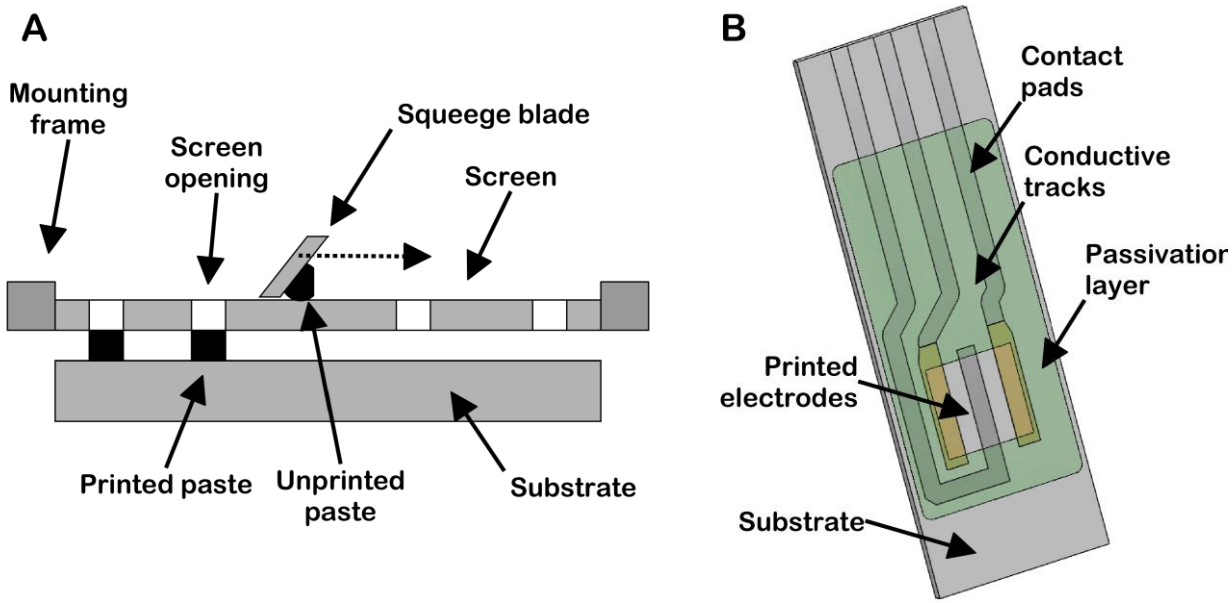

Figure 1.3. Schematic representation of (A) a screen-printing process and tooling, and (B) a screen-printed biosensor.

1.5 Flexible printed circuit boards manufacturing

Printed circuit boards (PCBs), not to be confused with screen-printing, is a mature photolithographic manufacturing technology for defining conductive tracks for, and mechanically supporting, electronic components. A metalized dielectric board, most commonly Cu on glass-reinforced epoxy laminate (FR-4), is patterned by way of photolithography. That is, Cu plated boards covered with a photoresist is imaged through photomask containing the image to be patterned. A chemical rinse removes the unwanted photoresist, while the remaining photoresist protects the areas from being

etched away in the succeeding step. The etching step removes all unwanted copper, and leaves behind the desired pattern. Any excess photoresist is then chemically removed. The maturing of PCB technology has led to an astounding level of complexity, with functions such as tens of signal layers. One of those functions is the ability to manufacture thin, flexible PCBs, or flexible printed circuits (FPCs). The flexibility allows for conformal robustness, due to the board's ability to follow change in shape, and lends conformity to applications. It enables flexible electronics, and is therefore a choice candidate for the trend of wearable electronics, where a piece of electronics is strapped to and forms to the shape of the human or animal body to gain intel on physical and physiological parameters such as heart rate, movement and chemical markers. The thin substrate, often 100 µm or less, reduces its weight, making it an ideal payload for deployment by drone. Manufacturing houses often operate with 100 µm line width as the lower limit.

2 Fundamentals of electrochemistry

A wide definition of electrochemistry is the interchange between electrical and chemical energy [36]. For electrochemical biosensors we only concern ourselves with the interface consisting of an electrical conductor and ionic conductor (electrolyte), such as a graphite electrode in a saline solution (see Figure 2.1). The electrode, is meant to probe system and gather information about specific analyte levels or groups thereof. The electrode used for studying the system is most often referred to as the working electrode. An electrical signal may however not be read without a closed path, and hence at least one more electrode is needed to close the circuit, the reference electrode. The purpose of the reference electrode is to serve as a constant reference potential, to which the potential of the working electrode may be referred, and which ideally remains unaffected by the events at the working electrode. In cases where considerable amounts of current is flowing, a third electrode is used to divert the current, such that the reference electrode may operate unperturbed [37]. One exception to this nomenclature is when two identical electrodes are used conductometrically, in which case they are called an electrode pair, with no discrimination between the two. Figure 2.1 illustrates how the components of a conventional electrochemical cell (Figure 2.1a) may be compacted to a single entity, here exemplified by a screen-printed electrochemical cell (Figure 2.1b).

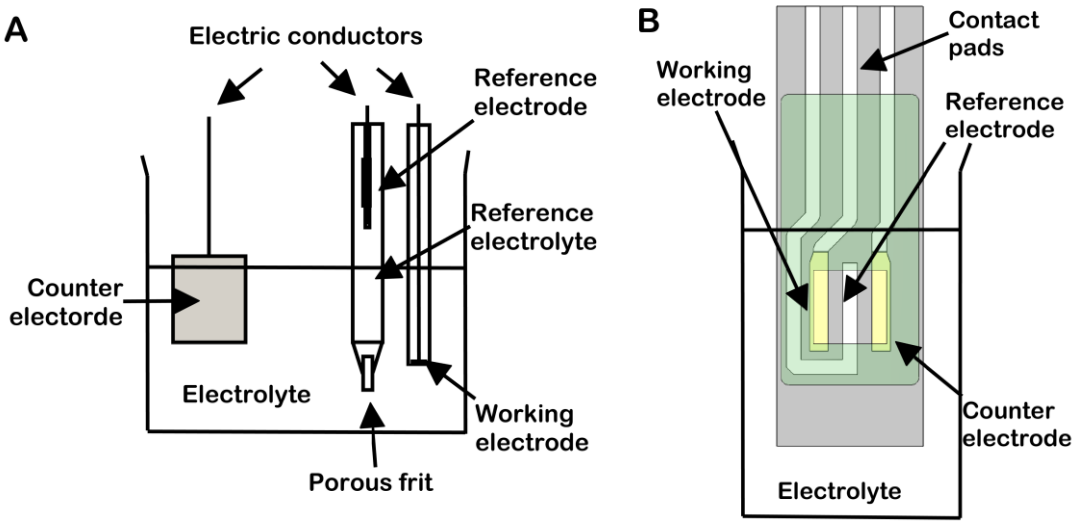

Figure 2.1. (A) Conventional and (B) integrated electrochemical cell in the form of screen-printed electrodes.

2.1 The importance of the reference electrode

Considerable attention has been dedicated to the reference electrode throughout this work. Although its function is well-known, it is sometimes overlooked in the literature supporting the field of analytical chemistry [38]. Authors generally seem to be satisfied that the sensor displays analytical responses proportional to the different analyte concentrations [39], [40]. The accuracy of this method, however, extends only to test matrices of well-defined composition.

The ideal reference electrode maintains its potential relative to the solution by an overall equilibrium equation with fast kinetics, making it highly non-polarizable. In practice it means that it is able to sink or source current without displacing its potential significantly. A good way to illustrate this is by I-E curves (current-potential curves). In these curves, the steady-state current response of a reaction is plotted against the poised potential, like the ones in Figure 2.2. The graphs represent two electrodes in a two-electrode mode. Their current responses are centered around the equilibrium potential for each respective reaction. The potential between the two equilibria is the open circuit potential (OCP), i.e. the potential measured when no net current is flowing

through the cell. Perturbation of those potentials results in an exponential current increase, following the behavior of the Butler-Volmer equation [41].

$$I = I_0 \left[\underbrace{exp\left(\alpha \frac{nF}{RT} (E - E_0) \right)}_{Anodic\ component} - \underbrace{exp\left(-\frac{nF}{RT} (1 - \alpha)(E - E_0) \right)}_{Cathodic\ component} \right] \quad (1)$$

Here, I is the current response of one electrode reaction based on the anodic and cathodic contributions (A). Their contributions are dictated by the difference between the externally applied potential E (V), and the equilibrium potential E_0 (V) of the electrode reaction, scaled by the charge transfer coefficient α, the number of electrons transferred per mole n, the faraday F (96 485 A s mol^{-1}), the ideal gas constant R (8.31 J K^{-1} mol^{-1}) and the absolute temperature T (K). The polarizability of the electrode reaction is largely given by the exchange current I_0 (A). The exchange current is the magnitude of the anodic or cathodic contribution when no net current is flowing, i.e, at the equilibrium potential. It contains information about the inherent chemical reactivity of the system, and depends on parameters such as chemical rate constants, quantities of the involved species, electrode material and composition, etc. The steeper the slope, i.e., the higher the exchange current, the better the reference electrode. In contrast, the working electrode often has a higher degree of polarizability provide a surface with a variable potential that is able to probe specific electrode reactions with high sensitivity. The reference electrode is less susceptible to polarization when the cell current is diverted through a dedicated counter electrode. However, in any real system there is always a small current drawn by the gate of the input transistor stage of the supporting instrument. This might cause a short-term offset, but can also lead to undesired reactions permanently changing the electrode, and consequently its potential over time.

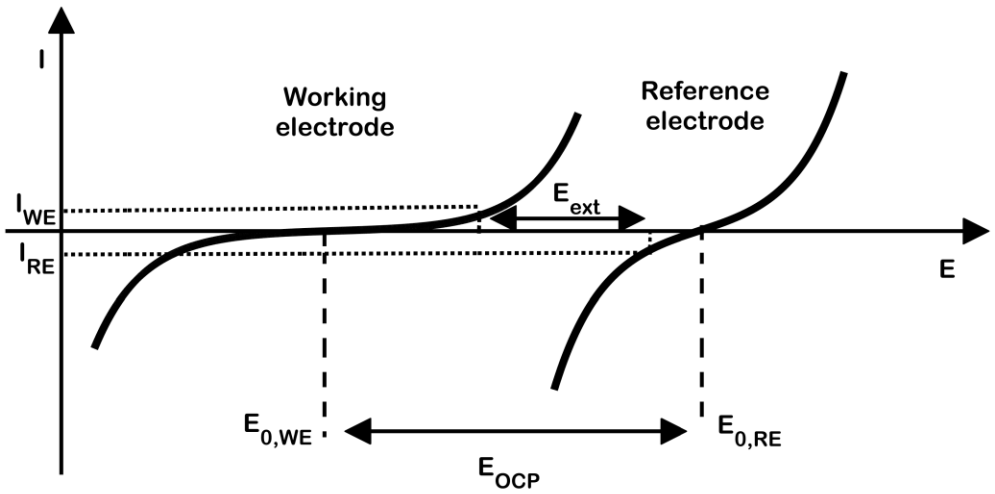

Figure 2.2. Representation of the current (I) responses to changing potential (E) for a working (WE) and reference electrode (RE) away from their equilibrium (E_0) in a two-electrode configuration.

Since the reference electrode potential is defined by its overall equilibrium reaction it is highly dependent upon the composition of the surrounding electrolyte. For laboratory use, the reference electrode commonly resides in a separate compartment where the electrolyte composition is maintained constant, and ionic contact is secured by a small porous frit or capillary. For compact and miniaturized systems, it is common to omit this reference compartment in favor of integration, making the reference electrode dependent upon the composition of the test matrix [42]–[44]. This construction is referred to as a pseudo-reference electrode. The true reference electrode may still be down-scaled from its laboratory design such that is not entirely at the mercy of the sample composition [42], [45]–[51], either by direct miniaturization, or by way of solid state reference electrolytes containing an excess of the reactants required by the reference electrode. Article III explores the usage of a NaCl-doped polyvinyl butyral as a solid state reference electrolyte immobilized on a screen-printed Ag/AgCl electrode.

Another performance parameter of the reference electrode is its stability over extended periods of time [44], [52], [53]. Even though the electrolyte composition may stay constant for a given application, there may be adverse reactions and effects influencing the potential that are not visible on a short timescale. Among these effects are

restructuring of the electrode, specific adsorption and desorption, corrosion, oxide formation, interdiffusion, electrodeposition and gas evolution. For autonomously operating sensor platforms that may be remotely located or otherwise hard to access, this behavior should be characterized, such that a significant change in sensor performance may be accounted or corrected for. Article I specifically addresses the issue of long-term stability, while Article IV deals with more immediate effects causing shift in operating potential.

2.2 Electrochemical instrumentation

The most fundamental piece of instrumentation for electrochemistry is the potentiostat. Its purpose is to maintain a given potential between the working and reference electrodes. Schematically (Figure 2.3) it does so by trying to equalize the potential difference between the reference electrode (-) and the working electrode and any added external potential (+), at the input terminals of a control amplifier. The amplifier corrects for the difference by supplying a current through the counter electrode. That current has to be the same one going through the working electrode, since the reference electrode is connected to a high impedance terminal (-). That current is the readout signal and is directly linked to the processes occuring at the working or counter electrode.

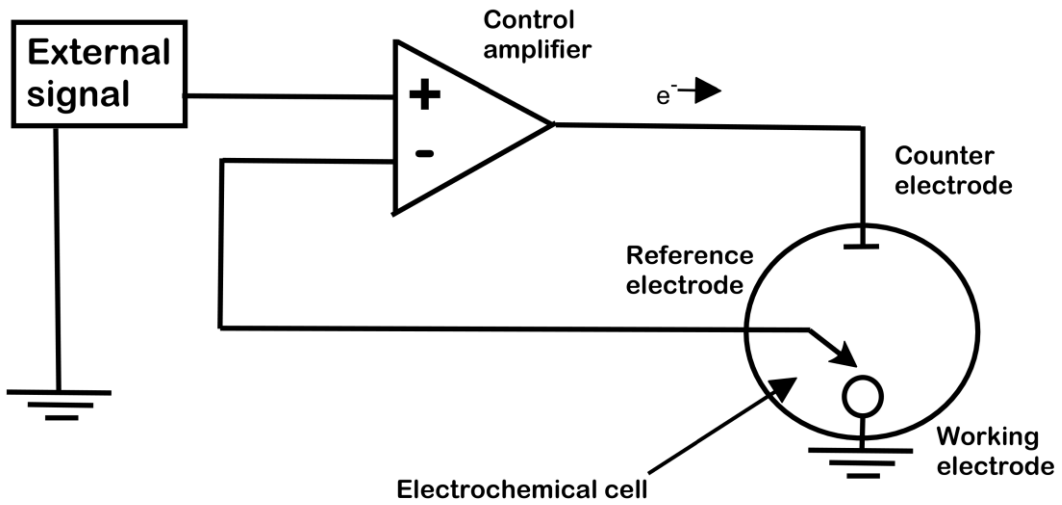

Figure 2.3. Schematic representation of a potentiostat circuit.

A galvanostat does the opposite, as illustrated in Figure 2.4. The current is maintained at a preset value whereas the potential between working and reference electrode (E) is the response. The current is directly supplied through the working electrode by a constant voltage source (V_{in}) and variable resistor (R). The following electrochemical techniques use has a galvanostatic or potentiostat circuit as part of the controlling circuit.

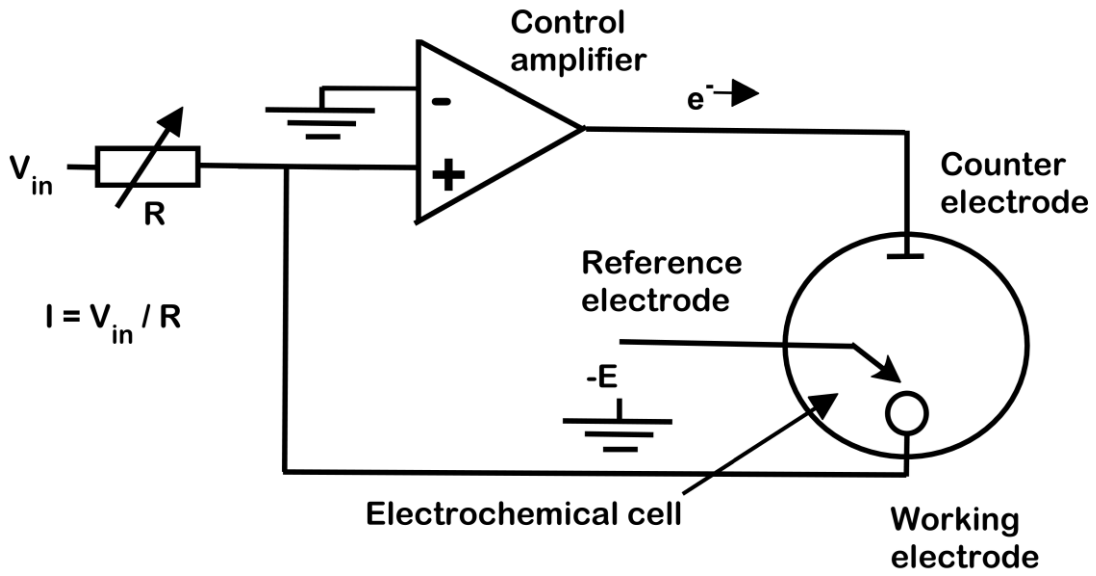

Figure 2.4. Schematic representation of a galvanostatic circuit.

2.3 Electrochemical detection techniques

The following section elaborates on the instrumental modes relevant for this thesis, and how they are employed in sensors. The nomenclature of electrochemical detection techniques may either refer to the electrical stimulus and response (instrumental mode), the mechanistic nature of the assay, or both. For example, an *amperometric* sensor is an electrochemical sensor where the electrical readout is an electrical current. An *aptasensor,* on the other hand, describes how aptamers are used to functionalize the sensor to be specific towards a certain analyte, without revealing what instrumental mode is used (it might even be non-electrochemical!). The perhaps most descriptive

would be to include both instrument mode and mechanistic principle in the name the technique. One example where both are used is in *adsorptive stripping voltammetry*. Adsorptive stripping refers to the removal of adsorbed species on an electrode surface. The way by which they are removed is by means of voltammetry, which refers to the electrical conditioning and readout of the sensor, further described in 2.3.3. For this section, the subsections are divided into instrumental modes. Within each subsections examples are given of what mechanisms are commonly used with the respective instrumental mode.

2.3.1 Amperometric biosensors

As previously stated, the term amperometry strictly means any experiment where the current is the response. In electrochemical biosensors, this technique is mainly used for monitoring the current response at a controlled potential step. The potential is maintained by the means of a potentiostat. The term chronoamperometry is often used to emphasize that the amperometric response are studied with events in time, such as titrations or potential steps. Potential step amperometry is perhaps the most common mode of operation for electrochemical biosensors, much owed to the success of glucose test strips for diabetes monitoring [54], and the simplicity of the technique. The voltage is simply stepped to a potential different from the open circuit potential (no current flowing) and kept there for the duration of the measurement, as illustrated in Figure 2.5.

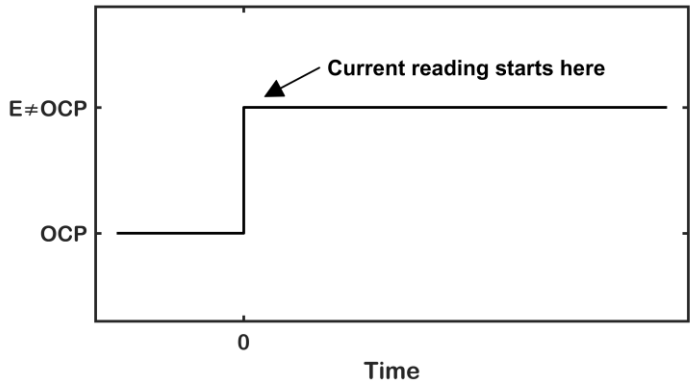

Figure 2.5. Potential step amperometry. The operating voltage is being stepped from the open circuit potential to a different value, and the current is being recorded from just after the step.

Whenever the assay involves an electrochemical reaction which can generate a measurable current when supplying the needed level of energy in the form of an electrochemical potential, amperometry may be used. There may be any number of chemical steps preceding this reaction. The most known examples are enzymatic sensors that employ oxidoreductase enzymes, where one of the reaction products is the electroactive product H_2O_2. A few common examples are glucose oxidase, lactate oxidase, choline oxidase and alcohol oxidase, for measurement of glucose, lactic acid, choline and ethanol in the bloodstream. The H_2O_2 is readily electrooxidizable at a +650 mV vs. a Ag/AgCl reference electrode immersed in PBS (phosphate buffered saline) containing about 150 mM of Cl^-.

2.3.1.1 Diffusion control, kinetic control and mixed mode

The amperograms in Figure 2.6b illustrate three different amperometric responses to a potential step, and is an function of the concentration profiles of the electrolyzed species (Figure 2.6a). A reaction can be diffusion controlled (--), meaning the electrode reaction is sufficiently efficient to deplete the reactants at the interface, and the transport of reactants to the interface becomes the rate determining step (RDS). Although there are other modes of mass transport control, such as migration of charged species in electric fields, or convection, diffusion is the most common limitation [55].

Under the condition of diffusion control, the current may be described by the Cottrell equation [55], or variations thereof:

$$I = nFAC^0\sqrt{\frac{D}{\pi t}} \quad (2)$$

where t is the time dependency (s), D is the diffusion coefficient of the relevant species ($cm^2\ s^{-1}$), A is the electrochemically active area of the electrode (cm^2) and C^0 the bulk concentration of the species (mol L^{-1}) before the potential step. This can be realized by manipulating the electrode potential to a region with high current, choosing an electrode, a catalyst, that is especially effective in facilitating the reaction, or work with low analyte concentration such that its heterogenous depletion is faster. This type of response is often utilized by disposable sensors, the transient signal obtained containing the necessary analytical information [56]. In contrast, for continuously operated sensors, this time dependence is sought removed. By moving the voltage to a region with lower currents, choosing a poor catalyst, or working with highly concentrated analytes, the current generated may solely depend on the electrode kinetics:

$$I = \frac{nF^2}{RT}AkC\left(E - E_{eq}\right) \quad (3)$$

where C is the analyte concentration at any given time (mol L^{-1}), and k is a parameter that quantities the sluggishness of the electrode reaction (cm s^{-1}). One thus arrives at an expression where the single variable is the concentration of the analyte, provided the potential is maintained constant. In reality there are often contributions from both kinetically (··) and diffusion controlled (--) modes. This is known as mixed mode (-·), where the current is in dictated by electrode kinetics, and in part by the concentration gradient. Decomposing the different contributions of a mixed mode response is a cumbersome exercise, and is avoided when possible. Engineering a kinetically controlled sensor is however seldom practically feasible since the electrode material itself is often not selective enough to the targeted analyte and one is rarely interested in merely high analyte concentrations. The recognition element that ensures analyte specificity added

to the electrochemical transducer sometimes act as an obstacle and moves the response toward a mixed mode. Adding to that, it is common to include multiple layers to achieve various traits, which could further complicates the mathematical description. One example of such a functional layer is the use of ionomers, a polymeric compound that promotes the transport of either positively or negative charged species, to block electroactive species that may interfere with the desired signal. The cationomer Nafion(R) is frequently used to limit the influence of negatively charged interferents such as ascorbic acid and acetaminophen (paracetamol) on the signal of blood glucose sensors [57]. In order to get back to the desired time-invariant, linear expression, one can limit the reactant flux by applying another functional layer, a mass transport limiting membrane. In this way one can establish a near-linear concentration gradient, so that the time dependence again disappears from (2) [58], [59]:

$$I = nFAk_mC \qquad (4)$$

where k_m (cm s^{-1}) is the mass transfer coefficient describing the slope of the linearized concentration gradient. This is frequently exploited in continuous mode sensors, such as continuous glucose sensors. The trade-off is an overall lower signal strength. Figure 2.6C shows an idealized response to stepwise titration of the analyte, which may represent either equation (4), or (3) under constant E, whereas Figure 2.6A shows the concentration profile (-) for one such step.

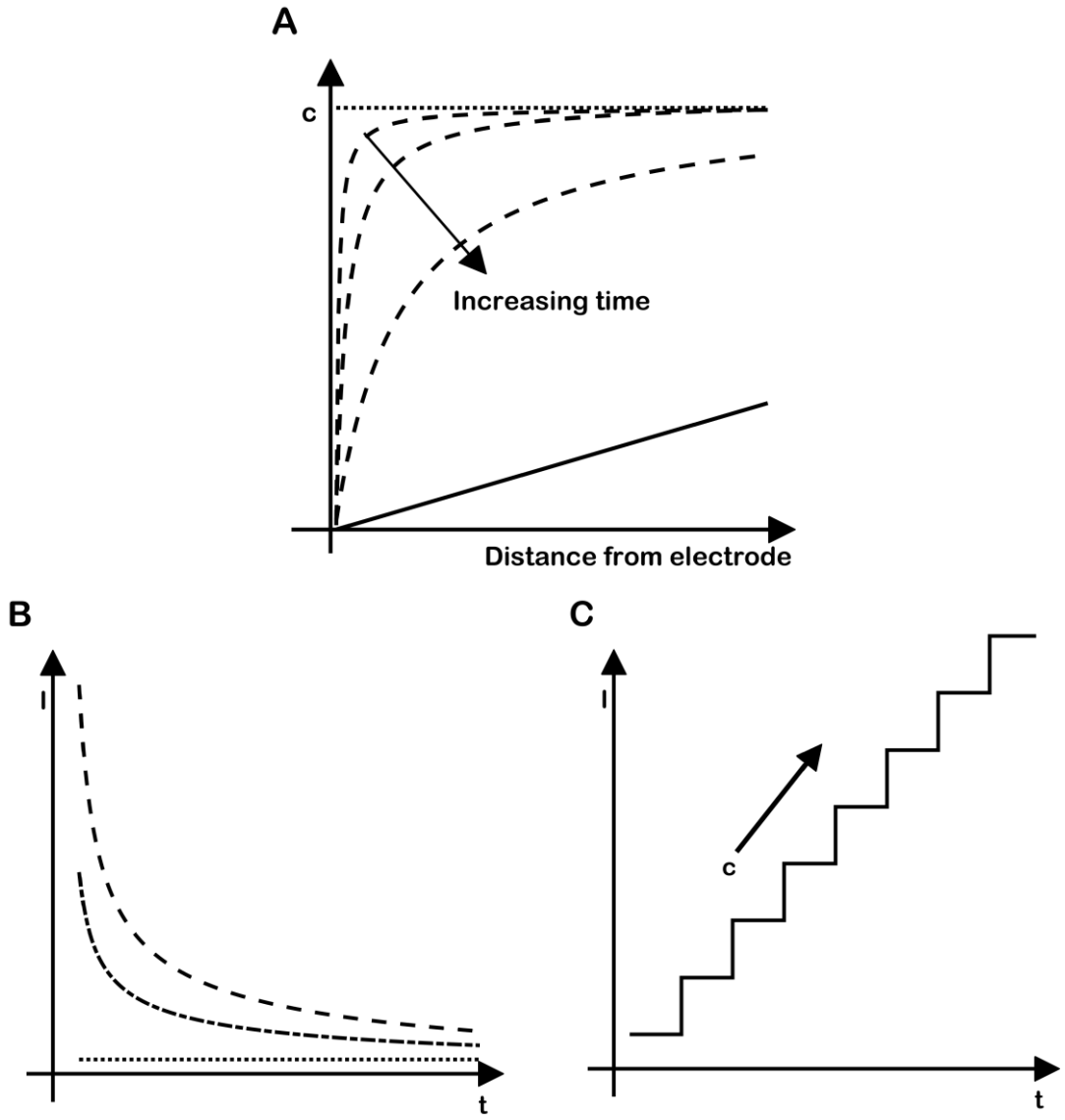

Figure 2.6. (A) Concentration profiles and (B) their corresponding potential step responses for diffusion controlled (--), kinetically controlled (··), mixed mode (-·). (C) Chronoamperogram for kinetically limited electrode reaction for increasing analyte concentration.

2.3.1.2 Multistep amperometry

One sub-form of amperometry is multistep amperometry (MA). Here, the working electrode is stepped between two or more potentials to probe different reactions [60]. It is particularly useful when one potential is used to set in motion a sequence of reactions, and a different potential is used to quantify a product of one of the successive reactions. During the preparation of Article II, multistep amperometry was sought to

replace a more advance technique, voltammetry, to interrogate the different chemical states of capsaicin adsorbed on a carbon electrode by a simpler technique [61]. Figure 2.7A shows how the current magnitude and sign changes with the different potentials, and that the magnitude is proportional to the concentration of capsaicin. The problem is that one cannot be absolutely certain that the responses solely belong to the desired chemical transformations. This is evidenced by performing the same measurement on a model redox compound, Figure 2.7B. Whereas the particular shape of a voltammogram may serve as a fingerprint of the molecule, multistep amperometry requires isolation of the chemical of interest to assure that the correct reaction is the one being targeted. Multistep amperometry was therefore not capable of replacing the more advanced technique in this instance.

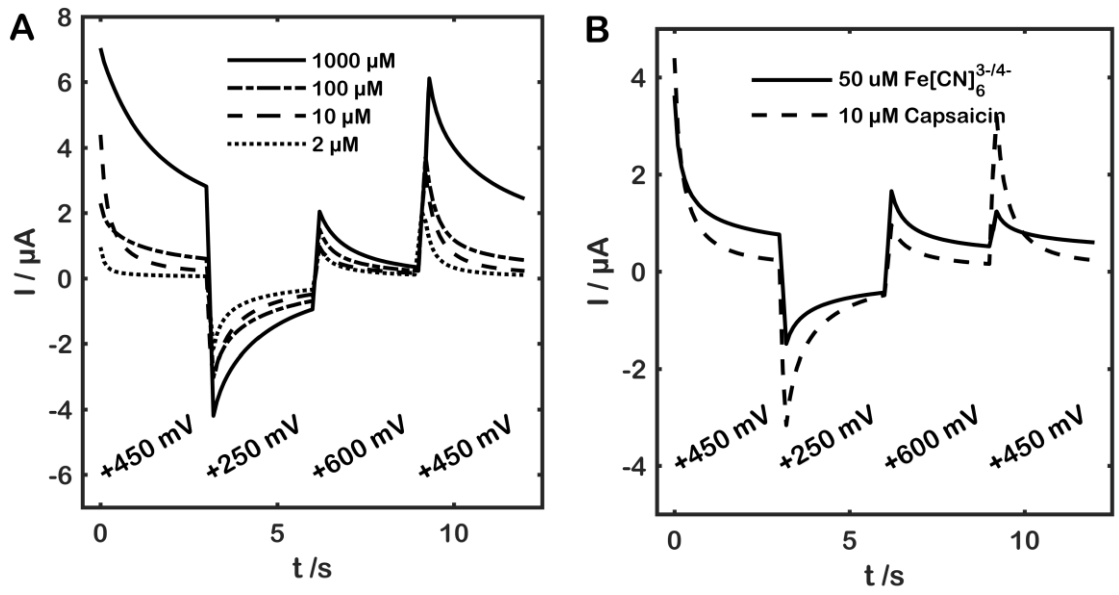

Figure 2.7. (A) Multistep amperometry for the detection of capsaicin. (B) Multistep amperometry of model redox compound (--) compared to capsaicin (-).

2.3.1.3 Squarewave amperometry

Article III employs a rarely used technique called squarewave amperometry (SWA), invented in 1982 by Brian G. Cox [62]. In this technique, two identical, ion-sensitive electrodes are cycled between two potentials, one above, and one below the reversible potential of the ionic redox reaction (0 V). The waveform is illustrated in Figure 2.8A for

four decades of the analyte concentration. The redox potentials corresponding to the different concentrations are indicated versus a fictive SHE. The ionic compound, e.g. an anion (A^-), may then be alternately oxidized and reduced:

$$A + e^- \rightleftharpoons A^- \quad (5)$$

If the frequency of the squarewave is sufficiently high, the oxidized form will not have sufficient time to diffuse away from the electrode, and is immediately reduced when the sign of the applied potential flips. After a few repetitions one may create two current decays of equal magnitude, and opposite signs, as displayed in Figure 2.8B. The cycles are needed in order to electrolyze any interferent species. The resulting signal may be used analytically. Furthermore, the absence of a reference electrode permits operation in unknown sample compositions.

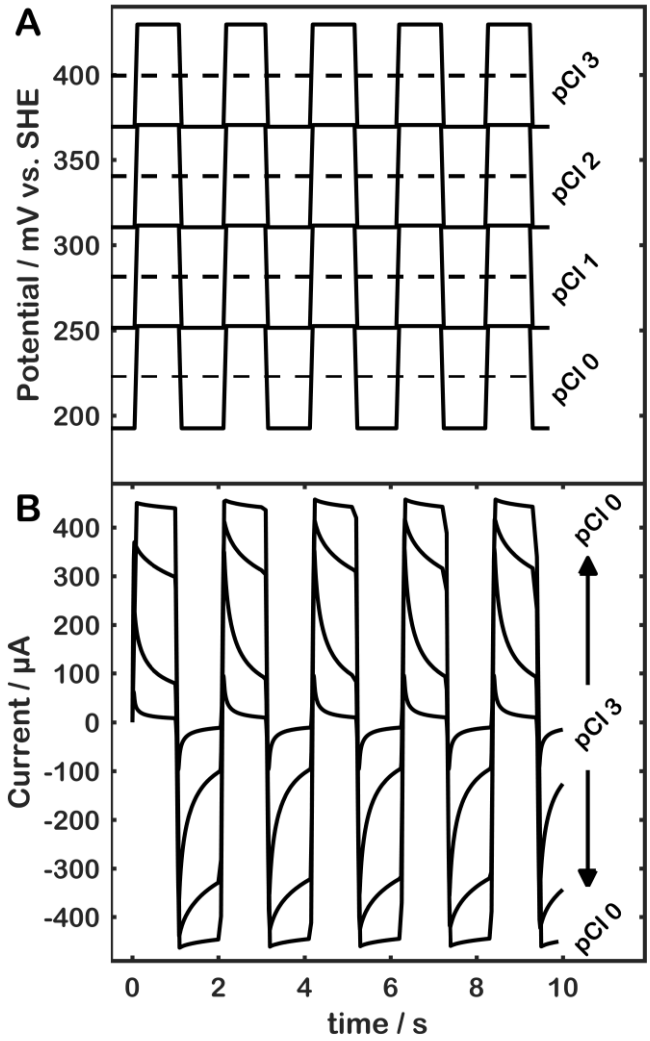

Figure 2.8. Theoretical (A) stimulus and (B) response for squarewave amperometry on Cl^- ranging pCl 3 to pCl 0. The dotted lines indicate the potential of the reference electrode relative to vs. SHE.

The technique has not been commonly used since the 1980s. This is possibly due to the focus on the detection of trace amounts of analytes, and the lower limit of detection (LOD) having become a strong figure of merit for analytical assays. While squarewave amperometry gives up to a 1000-fold higher sensitivity for ion detection compared to potential step amperometry, the background current caused by non-faradaic contributions prevents a low LOD (< 10 µM) [63]. It is however suitable for detecting analyte concentrations spanning several decades. In Article III, screen-printed Ag/AgCl electrodes are used for the detection of Cl^- in the range pCl 3.0 to pCl 0.0 using

squarewave amperometry on the flexible electrochemical sensor platform. A third Ag/AgCl electrode is used to provide a reference potential unperturbed by the reactions at the working and counter electrodes.

2.3.2 Potentiometric biosensors

In potentiometric sensors, a potential difference between two electrodes is the response, whereas the stimulus may be a controlled current, or the absence of one. In the former situation, the potential is adjusted to accommodate the preset cell current. The potential is characteristic of the electrode reaction(s). In order to maintain the current, the depletion of reactants will cause the potential to shift to other redox potentials rather abruptly. This tends to cause less predictable, non-faradaic contributions throughout the measurement, and hence works best with well-defined systems [41], [55]. For most biosensors, a well-defined system is a commodity, as cost is more important than accuracy, and the sample matrices are often complex in their composition. One sub-form of potentiometry favored by biosensors is that of open circuit potentiometry (OCP), and is often ambiguously used with potentiometric biosensors. It is a high impedance reading, meaning no appreciable current is flowing. The signal comes the exchange currents of the electroactive species at the interface, and consequently the relative concentrations of each participating redox couple. The OCP hence reflects the tendencies of the electroactive chemical species to react with electrode and may sometimes serve as an indicator of the stability of the system [64]. Since there is no current flow, there is no electrochemical depletion of reactants at the electrode surface, allowing for use in less well-defined systems. A potentiometric readout instrument can be realized with few components, such as a single chip instrumentation amplifier; a differential amplifier with impedance matching input stages. Since there is virtually no current draw through such a circuit, the technique is highly suitable for portable devices where the energy source is of limited capacity.

OCP mode is commonly employed in ion-sensitive electrodes (ISEs), i.e. electrodes modified with a recognition element that targets specific ions. Some examples are ill-

soluble silver salts, such as AgI, which have an affinity towards their dissolved ionic (I^-) species [44], [47]. Another group is that of metal oxides, e.g. RuO_2 and IrO_2 that are highly sensitive to H^+. More intricate modifications involve biological species like ionphores; lipophilic structures that promote the flow of specific ions. Ionophores exist for a range of ions, including K^+,Na^+,Ca^+ and NH_4^+.

In Article III, OCP is employed for the determination of pH. A carbon working electrode was employed in conjunction with the electrochemical sensor platform's OCP mode, further described in 3.2. Graphene oxide drop cast on the working electrode was used as the pH recognition element. A sensitivity of -26 mV pH^{-1} was achieved in the range pH 10 to pH 2.

2.3.3 Voltammetric biosensors

Voltammetry is a valued characterization technique for electrode systems that can yield information about both electrode kinetics and processes, as well as transport properties. The current is studied as a function of a potential sweep. The resulting I-E curve is an electrochemical spectrum indicating at which potentials different processes are occurring [55]. The most common voltammetric mode is that of cyclic voltammetry (CV). Here, the potential waveform is a high amplitude (100s of mV), low frequency (< 1 Hz) sawtooth waveform [55]. The most recognizable feature is the duck-shaped voltammogram that comes from the electrolysis and diffusion of the well-behaved reversible redox species (see Figure 2.9a). The curve starts off at a potential where no significant electrolysis is occurring, and hence no net current is flowing. As the potential is swept more positively, the rate of oxidation increases in line with the anodic term of the Butler-Volmer equation, resulting in an exponential increase. The increase eventually decays as the reactant (R) is depleted and moves into a Cottrellian type response. When the sweep direction is reversed, the oxidation current further decays with the potential and eventually moves on to reducing the product of the oxidation (O), and the exact same events are repeated. As the processes involved become more numerous and different in nature, their responses superimpose, and become more

demanding to deconvolute in order to extract any meaningful information (see Figure 2.9b). These processes may range from electroreduction- and oxidation, diffusion, ad- and desorption or gas evolution, and may depend on preceding and succeeding electrochemical and chemical reactions. Although initially a characterization technique, the voltammetric method is now employed analytically. Presumably, this is in part owed to increased availability, functionality and affordability of electrochemical workstations, and in part more sophisticated data analysis software packages capable of extracting meaningful, analytical data. Analytical information may be extracted from peak potentials, peak height or charge.

2.3.3.1 Squarewave voltammetry

There are many other sub-forms of voltammetry, the common denominator being changes to the potential waveform in order to achieve certain advantages. One which is particularly popular in analytical applications is that of squarewave voltammetry (SWV). Similar to CV, a linear ramp - or more accurately linear staircase due to the digital nature of all modern instruments - is the base waveform. A squarewave signal is superimposed on the base waveform, as illustrated in Figure 2.9c. The overall effect is an alternating interrogation and relaxation of the concentration gradient, which in most cases produces a higher signal, lower nonfaradaic contribution and ultimately a sensor with higher sensitivity and limit of detection compared to CV. The squarewave current is the difference between the current obtained at each half-period of the squarewave In Figure 2.9d, the responses of squarewave and cyclic voltammetry are compared under equal conditions. The peak height of the squarewave voltammetric signal is much more prominent than that of cyclic voltammetry. Squarewave voltammetry typically has a much higher baseline signal than cyclic voltammetry due to the two components of the squarewave current often being of opposite sign, and the signal is commonly postprocessed using baseline corrective algorithms [65].

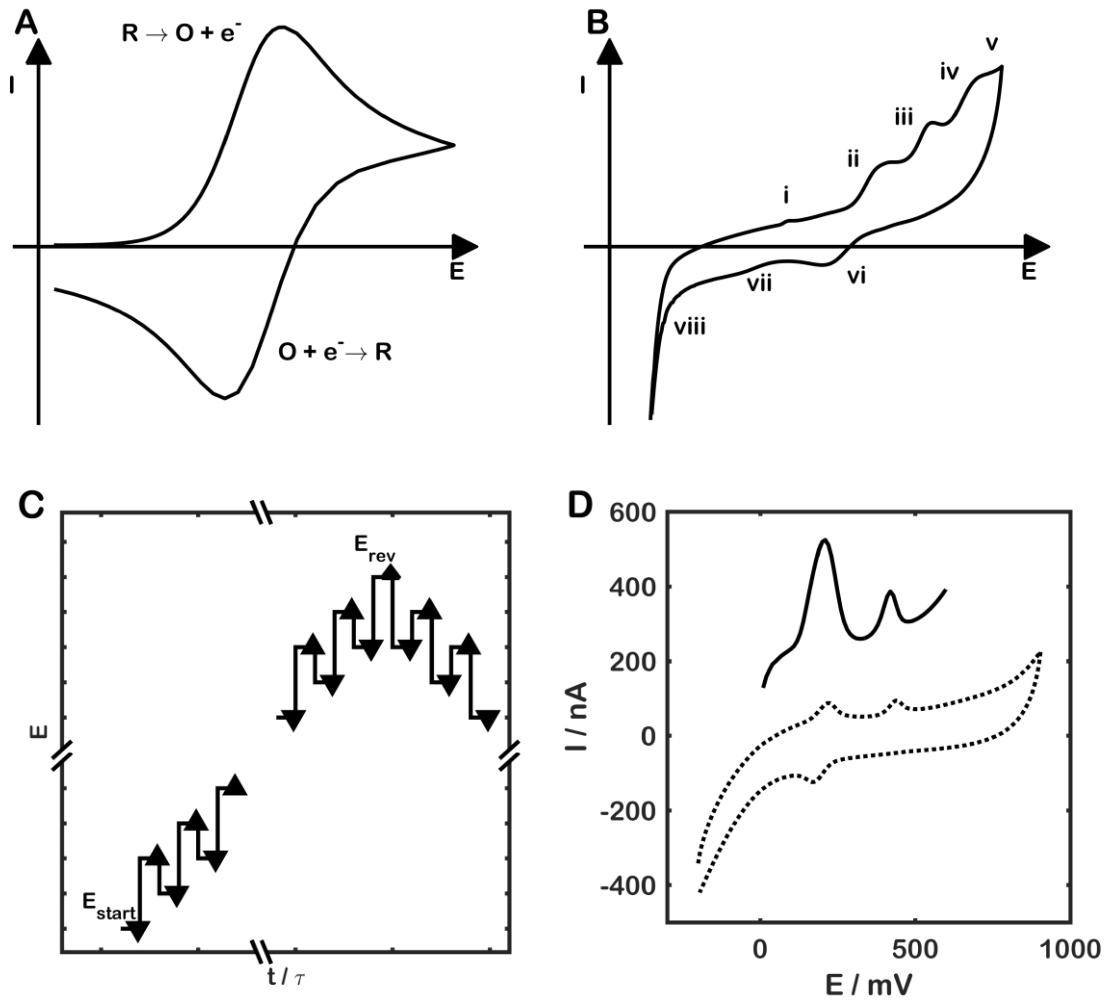

Figure 2.9. Cyclic voltammograms of (A) reversible redox couple R and O, and (B) voltammogram with eight observable processes. (C) Potential waveform of squarewave voltammetry. The forward (▲), reverse (▼) currents are sampled just before the next potential step. (D) Comparison between cyclic voltammetry (··) and squarewave voltammetry (-). The squrewave current is the difference between the forward and reverse current.

Article II employs a crude form of squarewave voltammetry, and also includes the backscan completing the cycle. The modification was coined coarsely-stepped cycle squarewave voltammetry (CCSWV). Since the electrochemical sensor platform has a minimum potential increment of 60 mV, it is a coarser setting than commonly used for this technique (<20 mV). Smaller squarewave amplitude is usually preferred due to the reduced risk of neighboring peaks merging [65]. In spite of its lack of highly resolved potential steps, it was able to detect capsaicin with a LOD of 0.81 µM, which is comparable to that of cyclic voltammetry (0.48 µM).

2.3.4 Impedimetric biosensors

In electrochemical impedance spectroscopy (EIS), the electrical stimulus is most often a small amplitude (a few tens of mVpp) sinusoidal waveform superimposed on a direct current (DC) signal. When the DC potential is centered at the equilibrium potential of the reaction under study, that AC potential perturbs the equilibrium, but only within the linear region of the IE curve. The system may thus be described linearly, which makes it possible to mathematically model. The relationship between the current and voltage is best described by impedance. The AC waveform is swept in frequency in order to gather information on the rates of the different processes involved. The frequencies may range from a few mHz to hundreds of MHz. The impedimetric response is most often illustrated by Nyquist plots (Figure 2.10A), presenting the real and imaginary components of the impedance for different frequencies, or by the absolute impedance and phase versus the frequency log-log plot in a Bode plot (Figure 2.10B). Commonly, the raw data is supplemented by an equivalent circuit model, both to verify the different processes and to extrapolate important parameters such as charge transfer resistance, solution resistance and double layer capacitance. Sensors employing some form of this technique are often referred to as impedimetric or conductometric sensors. EIS shares the historic development of voltammetry by initially being an electrochemical characterization technique, but has increasingly been used for sensor applications [66], although not yet to the same extent as CV. The technique relies heavily on precision instrumentation, including potentiostat, signal generators and phase analyzers. These factors along with extensive use of mathematical theory, presently makes the technique less popular than voltammetric sensors. One of its practical advantages is its ability to interrogate a process with small perturbations, making it less taxing for the electrode, and as a result increases its lifetime.

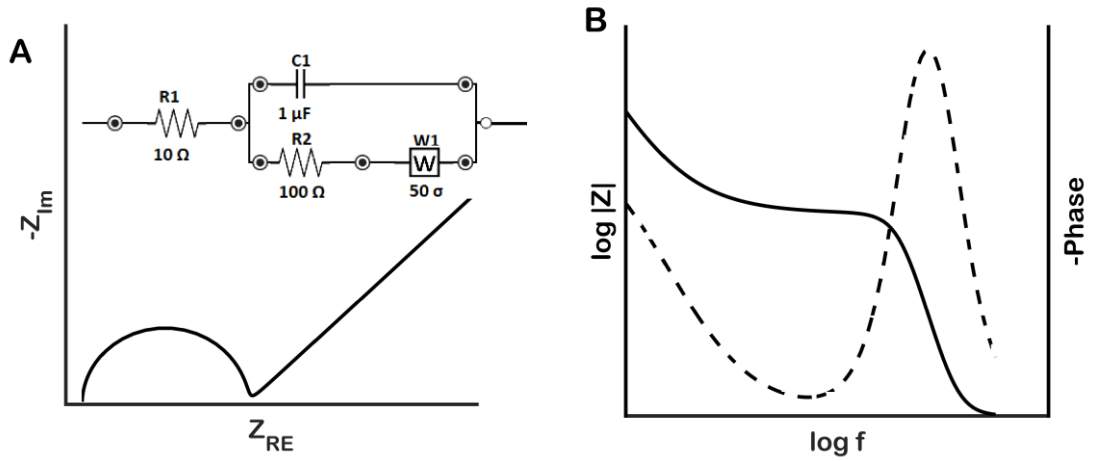

Figure 2.10. (A) Nyquist plot and (B) bode/phase plot. The inset shows the equivalent circuit for the system.

2.4 Simulation in electrochemistry

Simulation is a powerful tool and has quickly become an incorporated part of the workflow of microsystem design and analysis [67]. Simulation sometimes eliminates the need for iterative loops of design, manufacturing, testing, analysis and re-design by allowing the prediction of the system response under different parameters. Mathematical modelling has been an important part of electrochemistry since the early days [36]. In the age of the computer, numerical simulation is playing an increasingly extensive role. Numerical simulation methods, such as the finite difference method (FDM), or finite element analysis (FEA), are especially useful when the problem does not have a well-defined analytical expression or solution, or for multi-dimensional solutions [68]. Numerical simulation, in addition to being used for design optimization, is also useful for understanding and visualizing physical processes. It is however often limited to subsystems, as the number of intercoupled physics, heterogeneity, size and general complexity of the system becomes too demanding for modern computer systems [69].

In electrochemistry simulation is particularly useful for isolating the processes of one electrode interface. This is experimentally impossible due to the need for a closed circuit to gain any kind of readout, and hence a second electrode interface is introduced [38]. One of the challenges with electrochemical simulations is the extensive use of planar geometries (~cm) that have a low degree of symmetry, coupled with steep and narrow concentration gradients (< 1 µm) and dynamic, time-dependent techniques. Personal computers cannot render simulations under these conditions with sufficiently high accuracy, and one has to resort to cluster computing [70]. However, if the geometry can be simplified, the size of the model becomes manageable for personal computers within a reasonable timeframe (hours). One electrode geometry that lends itself particularly well to simplification is an electrode microarray, a small unit electrode repeated in two space dimensions. Here a single electrode can be simulated, and the array effect is gained via symmetry couplings to its neighbors. Furthermore, circular unit electrodes can be collapsed into the 2D cross-section of a cylinder, and revolved to extrapolate the full-scale result, which have proven to match experimental data quite well [71], [72].

Highly symmetrical designs may however not always be practically feasible for a given application due to physical limitations such as as size and shape.

2.4.1 The current state of simulation in electrochemical biosensors

In an effort to check the current status of simulating complex electrode geometries, seven years after the above claim was made, we simulated cyclic voltammetry on a planar spiral electrode. The end-goal was to investigate the chemical cross-talk between three parallel electrodes coiled in a spiral. This piece of work was considered by the authors not to be sufficient for a standalone research paper, and is hence adapted for this thesis.

Spiral patterns is one way of compacting long band electrodes in order to acquire a smaller footprint. Since the number of neighboring electrodes increases with each revolution, the effect of chemical cross-talk may become more prominent. This may produce adverse, unwanted effects such as reduced sensitivity and selectivity, or it may increase the response due to recycling of the reaction products, so-called redox recycling [73], or there might not be a discernable effect at all. Additionally, if the band electrodes are sufficiently narrow, they may benefit from radial diffusion profiles, and thus increasing the reactant and product flux, which in turn generates a higher sensitivity in a biosensor.

The geometry in the present simulation consists of a 200 µm wide electrode coiled in an Archimedean spiral:

$$r = a + b\theta \tag{6}$$

where r (µm) and θ (Rad) are the radial and angular polar coordinates, and a is the radial offset from the center that decides the pitch (µm), in case of parallel electrodes. This study was however limited to one electrode with $a = 0\ \mu m$, $b = 250\ \mu m$ and $0.35\pi < \theta < 4.1\pi$, creating a spiral of around two full revolutions and a geometrical area of 0.0418 cm^2, as depicted in Figure 2.11. The spiral was enclosed in a cylindrical

domain (r=4 mm). The height H (m) of the cylinder was set to 200 µm, which is well above a conservative diffusion length:

$$\mathrm{H} = 6\sqrt{Dt_{max}} = 6\sqrt{10^{-5} cm^2 s^{-1} \frac{\mathrm{E}_1 - E_2}{\nu}} \tag{7}$$

where D is the diffusion coefficient of the reactant species ($cm^2\ s^{-1}$) and t_{max} represents the length of the experiment (s), which is determined from the potential range scanned $\mathrm{E}_1 - E_2$ (V) and scan rate ν ($V\ s^{-1}$).

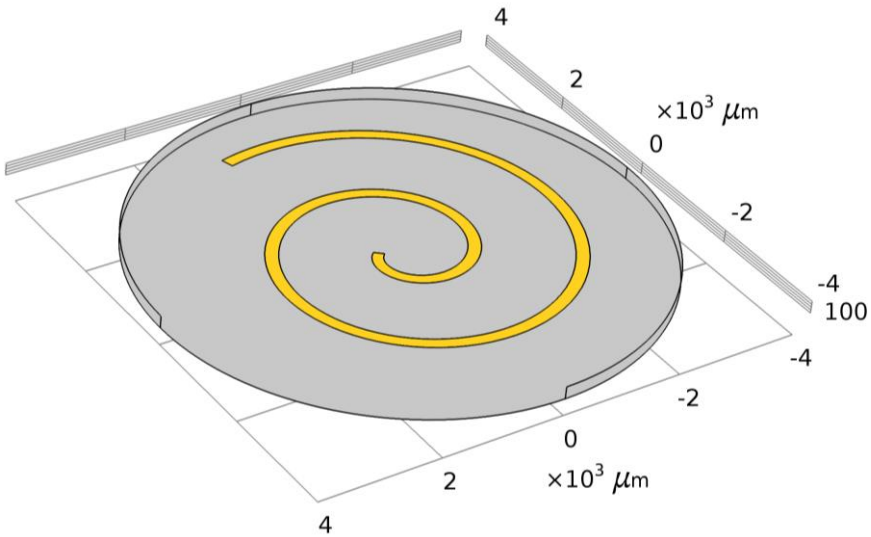

Figure 2.11. Geometry of single spiral electrode.

The simulation was carried out in the FEA software COMSOL Multiphysics' (5.3:249, COMSOL AB) electrochemistry module. The hardware used was a 3.5 GHz 6-core processor (Intel Xeon, 15 MB cache) computer system having 32GB of 2133 MHz error-correcting code memory. The mesh was set up to have the highest density close to the electrode surface, and diminish at a forced maximum rate into the bulk. The number of degrees of freedom arising from the granularity was kept below a limit that did not exceed the memory, which was found to be just above 5 million for this simulation. The electrode surface was built with triangular elements, whereas the surrounding bulk solution had a tetrahedral structure with . Minimum element size close

to the electrode (1.5 to 10 µm) and growth rate were varied (1.02× to 2×) until a healthy looking voltammogram was obtained. A typical mesh can be seen in Figure 2.12.

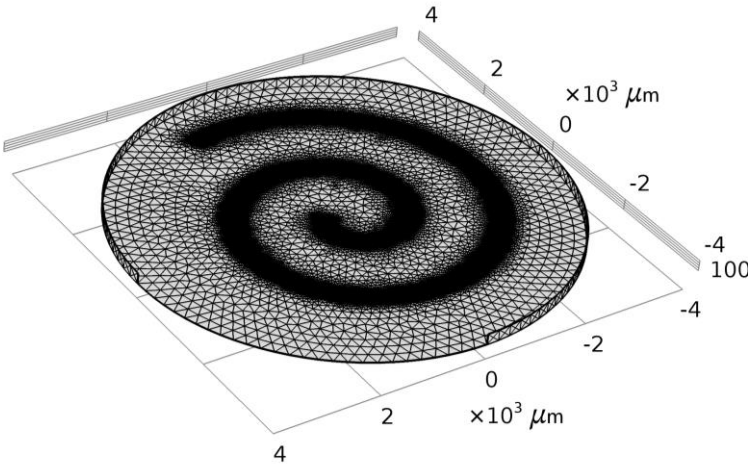

Figure 2.12. Typical mesh.

The electrode was set up for one-electron electroanalytical Butler-Volmer kinetics. This is a continuation of (1), which accounts for varying concentration of reactant species, C_{ox} (M) and C_{red} (M) by redefining the exchange current through a concentration independent rate constant; the heterogeneous rate constant k_0 (m s^{-1}):

$$I_0 = k_0 F A C_{ox}^{1-\alpha_c} C_{red}^{\alpha_c} \quad (8)$$

A cyclic voltammetry study was performed. The electrode potential was cycled between -200 and +200 mV. In order to limit the initial transient, which occurs because of an attempted division by zero due to the reactant being at zero concentration, the time stepping settings was changed away from the default settings for this mode. A strict backward differentiation formula with a forced initial step of 0.1 ms, followed by a maximum step limitation of 40 ms, with the number of orders set to 1. The remaining simulation parameters can be seen in the table below.

Table 2.I. Parameters for finite element analysis simulations

Parameter	Symbol	Unit	Value
Temperature	T	K	293.1
		℃	20
Faraday constant	F	A s mol^{-1}	96485
Ideal gas constant	R	J K^{-1} mol^{-1}	8.314
Heterogeneous rate constant	k_0	m s^{-1}	1
Initial oxidized species concentration	C_{Ox}	mM	0
Initial reduced species concentration	C_{Red}	mM	1
Cathodic charge transfer coefficient	α_c		0.5
Equilibrium potential for electrode reaction	E^0	mV	0
Start and end potential	E_1	mV	200
Reversal potential	E_2	mV	-200
Scan rate	ν	V s^{-1}	1
Diffusion constant for oxidized species	D_{Ox}	cm^2 s^{-1}	10^{-5}
Diffusion constant for oxidized species	D_{Red}	cm^2 s^{-1}	10^{-5}

The result of having insufficient granularity (Figure 2.13a) can easily be seen in the shape of the voltammogram, as anomalous spikes in Figure 2.13c. In this case the spikes appear in the depletion regions of the voltammogram, i.e. when the concentration profiles extends close to its maximum length into the bulk. This indicates that the mesh is not dense enough towards the bulk solution. The mesh that yielded the best parameters had a maximum element size of 3 µm on the electrode surface, and a 1.6× maximum growth rate (Figure 2.13b), giving 5.1 M degrees of freedom. It took 19h to resolve on the current computer system. This is without the additional electrodes to simulate the complete cell, and how the reaction products of each electrode reaction affect the neighboring electrodes. In contrast, the mesh in Figure 2.13a was set up with a maximum 5 µm element size, with a 1.8× maximum growth rate into the bulk. The resulting mesh gave 3.8 M degrees of freedom and solver time of 15 h.

The best voltammogram (Figure 2.13d) is not a perfect rendition of a 1D simulation due to it having some spikes at the extremes. It is however close enough to be considered for use in design optimization. The fact that the voltammogram takes on the characteristic duck-shape, and matches the 1D case, reveals that the electrode does not

benefit from radial diffusion under the current conditions, i.e. the perpendicular component of the diffusion dominates any parallel component. The simulation time however is impractically long for this isolated problem. The time would further increase when introducing more electrodes, reactions, physics, and variables. This leads us to believe that the claim made by Compton et al. still holds true, but that we are approaching something more practically useful in the not too distant future.

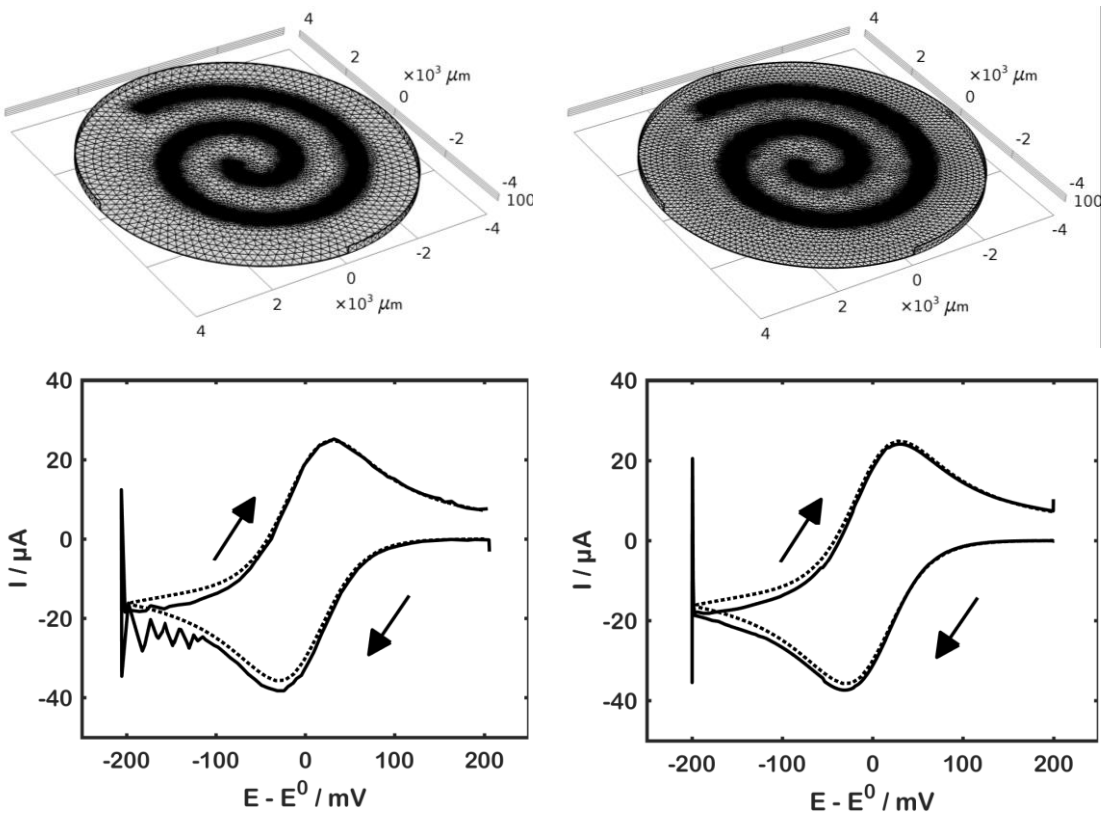

Figure 2.13. Meshes with low (A) and (B) high granularity, and (C-D) their corresponding voltammograms (-) compared to a 1D simulation (--).

3 Electrochemical sensor platforms

In recent years, electronics and computer programming have become more readily accessible to the public. Modern consumer electronics have developed low cost microcontroller platforms such as Arduino (Arduino LLC) and Raspberry Pi (Raspberry Pi fdn.), which can be coupled with simplified development environments and abstract programming to lower the threshold for the uneducated to embark on electronics projects. There is reason to believe that this development has benefited the science of microsystems and miniaturization in a way that makes it easier to demonstrate novel sensor and actuator schemes as compact and autonomous devices (rather than the isolated part connected to a benchtop instruments in a tangle of wires). New electrochemical biosensors are often reported in conjunction with a prototype measurement system in order to strengthen its validity in a "real" application, as encouraged by many scientific journals. Nyein et al. has in series of papers presented a flexible wearable sensor platform for multianalyte sensing of metabolites in skin perspiration with detachable sensors [10], [74]. The parameters monitored are Ca^{+}, lactate, glucose, K^{+}, Na^{+}, pH and temperature. The fact that the amperometric mode is tailored to sensors operating at 0 V vs. the reference electrode greatly simplifies the potentiostat design, resulting in a smaller component footprint and lower current consumption. On the other hand, it limits the platform to a certain sensor architecture that only operates at this potential: These sensors are produced by electrodeposition of a Prussian blue electron mediator, followed by drop casting of the enzyme solution. The process of electrodeposition is time consuming and harder to realize for batch production, since the working electrode of each individual sensor needs to be addressed, and treated equally. The fixed potential for this sensor platform also prevents the utilization of voltammetric methods. Martín et al. produced a similar device for monitoring glucose and lactate in sweat with screen-printed electrodes embedded in a sweat pumping microfluidic device, connected to a wearable flexible PCB [75]. To circumvent electrodeposition as a manufacturing technique, an ink containing graphite particles pre-modified with Prussian blue was used to define the working

electrode. However, no details of the PCB design and operation were disclosed. Other portable electrochemical platforms include glucose monitoring in tears through wireless contact lenses [76], NO, NH_3, fabric and tattoo sensors with integrated read-out circuitry and telemetry for pH, K^+ and NH_4^+, phosphate and glucose monitoring in saliva through a mouthguard with integrated sensor and instrumentation [77].

A few development projects for affordable and portable generic electrochemical instrumentation have been initiated [78]–[80]. Researchers from the University of California Santa Barbara presented an affordable (<$80), hand-held, open source potentiostat, the CheapStat, in that errand [81]. This was later succeeded by the Rodeostat, which is a shield for Arduino, with slightly better specs [82]. Another system, the PSoC-Stat, utilizes the programmable system-on-chip (PSoC) architecture provided by Cypress Semiconductor to make a single-chip potentiostat device from a pre-existing $10 development board (CY8CKIT-059) [78]. In short, configurable analog and digital blocks are programmatically strung together to perform the potentiostat function, all with a single integrated circuit. The general-purpose nature of the PSoC architecture means the analog components are not optimized for electrochemical instrumentation. Parameters like common-mode rejection, input impedance and leakage currents will affect its accuracy, especially at low current. The PSoC-stat currently needs to be powered through a computer, hence limiting its portability. A different group reported a hand-held, wireless and open source platform including wireless data transfer to smartphone [83]. These examples reflect the growing need and interest for small, portable and low-cost, yet universal instruments for electrochemical sensors.

All of these projects rely on interfacing with disposable screen-printed electrodes. While exchangeable electrodes are convenient for one-shot, disposable sensor applications, the electronic interface between sensor platform and sensor creates a point of weakness. The metal-metal interface is prone to corrosion, which will weaken the connection, and potentially induce additional impedance, adding error to the sensor readings. Having electrodes integrated in the same packaging material as the sensor platform would eliminate that junction. The current sensor platforms are in addition

somewhat limited by having rigid packaging. Especially in light of the massive growth in wearable electronics, mechanical flexibility makes for easier integration with such applications. Size and weight are also factors that cause limitations. A thin, flexible format would reduce the weight compared to a standard rigid PCB through a ten-fold thickness reduction, under the assumption that the base materials have similar masses.

Commercial suppliers have also caught on to the growing need for easy-to-use, portable instrumentation, although their prices do not differ significantly from laboratory equipment, costing at least $1000 [79]. The return for the investment are versatile instruments capable of many instrumental modes, with high accuracy and intuitive user interfaces, which are suited both for high precision laboratory work as well as in-the-field. They may however be too sophisticated for the end-product, and is not viable in a mass production context.

In summary, the work in this thesis seeks to improve upon existing, low-cost universal electrochemical sensor platforms by adding mechanical flexibility, size and weight reduction, integrated electrodes at a much lower material cost to than retail prices, and at the same time maintain versatility and universality through enabling multiple instrument modes.

3.1 The developed electrochemical sensor platform - ecFlex

The sensor platform (Figure 3.1, Figure 3.2, *Table 3.II*) resulting from the work described in this thesis, the ecFlex, seeks to improve upon some of the shortcomings of the state-of-the art standalone electrochemical sensor systems, while utilizing their strengths. Its component count is kept down both to limit the size and cost (~ €25 in 2018). See appendix A and B for schematics and bill-of-materials. A flexible format is used in order to provide physical versatility. In this way it can be attached to curved surfaces, and conform to motion, while remaining light (1.2 g). Mechanical design, electronics design, software and firmware code is made open to the public such that it can be further adapted towards specific applications through the links in Table 3.I.

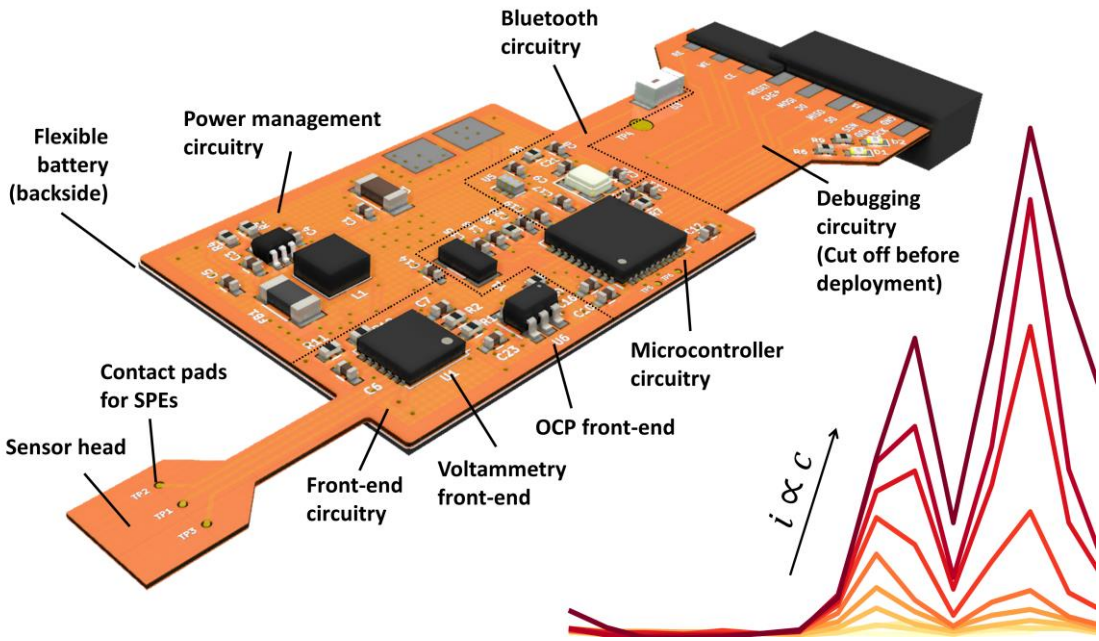

Figure 3.1. 3D model of sensor platform. The arrows indicate the main functional blocks.

Table 3.II. Sensor platform main components and technical specifications

Description	**Specification**
Overall weight	1.2 g
Overall size (peninsulas excluded)	29 × 25 mm
Supply voltage	Nominal 3 V, (2.7 - 5.25)
Battery life	Variable, depending on transmission rate, transmission power, mode of transmission (wired or wireless) 14 h (OCP or AD with cell current 2 µA, 500 ms transmission rate, BLE communication, 3V supply, 25 mAh battery)
Battery BV-452229-25ET (BrightVolt LLC)	Flexible, lithium polymer, thin-film battery that fits the physical dimensions of the PCB.
Microcontroller CC2540 (Texas Instruments)	Main controlling chip, integrated BLE module, integrated 12-bit ADC
Power management TPS61220 (Texas Instsruments Inc.)	Chip boost converter that regulates battery voltage and maintains the supply voltage
Voltammetry front-end LMP91000 (Texas Instsruments Inc.)	Chip for cell conditioning and current conversion for voltammetry modes.

OCP front-end MAX4461 (Maxim Integrated Inc.)	**Instrumentation amplifier chip for reading open circuit-potentials**
Screen-printed electrodes Custom	Electrodes that are printed in paste form onto the contact pads of the sensor heads and cured to form solid, electrochemical transducers. The materials are chosen depending on application
Debugging circuitry	Debugging lines for in-line code debugging and Bluetooth package intercept. This section also includes breakout for individually addressing each electrode, either for external electrode or instrument connection, and lines for SPI communication.

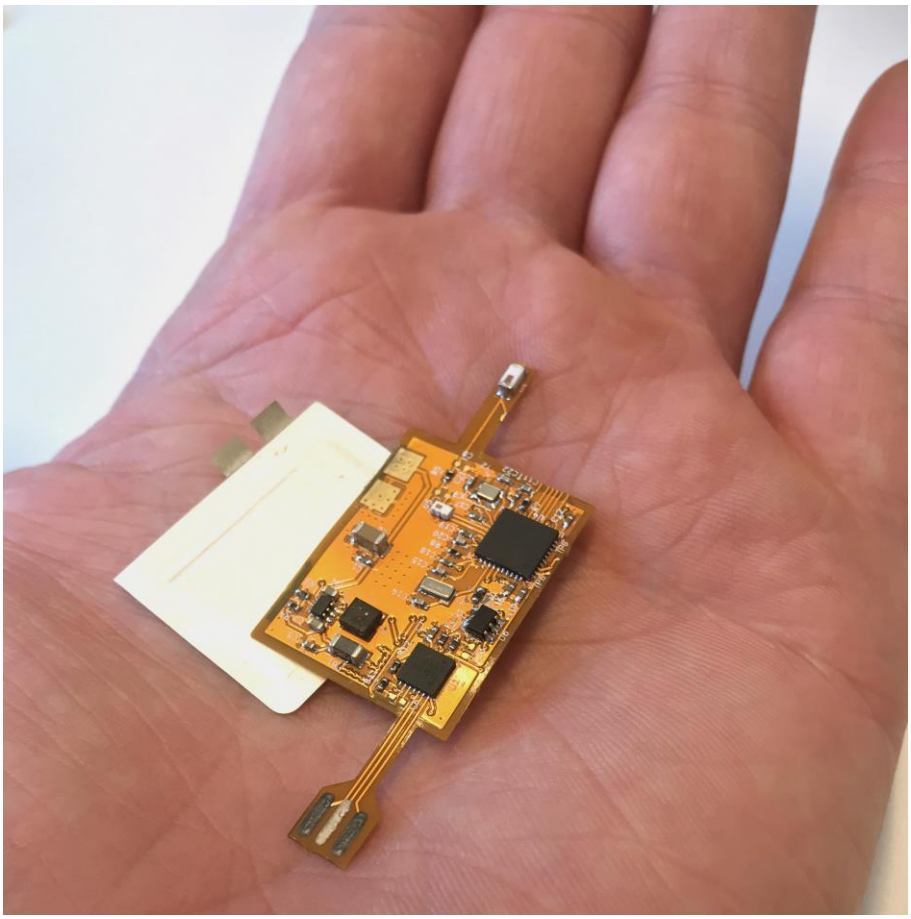

Figure 3.2. Picture of sensor platform with debug circuitry cut off and the flex battery that goes on the back.

Table 3.I. Links for design files of the electrochemical sensor platform.

Description	**Link**
Hardware design files, including mechanical and electrical	https://github.com/sindresops/ecFlex-HW
Firmware code	https://github.com/sindresops/ecFlex-FW
PC software code	https://github.com/sindresops/ecFlex-SW

3.1.1 Hardware design

The physical size of the sensor system is like many other similar applications dictated by the size of its power supply. A 25 mAh, 3 V flexible Lithium Polymer battery (BV-452229-25ET, BrightVolt LLC.) is used. This is currently the smallest, highest energy density flexible battery commercially available, measuring 29 mm × 25 mm × 0.45 mm. Its technology makes it non-flammable, and it can be cut in half without damage. The only effect is a shorter operational lifetime due to a comparable reduction in the storage capacity (although the interior will be exposed to the surroundings) [84]. It is situated on the rear side of the FPC. The platform thickness is defined by the FPC stack-up in Figure 3.3, which is a standard four signal layers with polyimide as the base material, and the thickness of the battery. This totals to around 760 µm, disregarding the discrete components distributed around the top side.

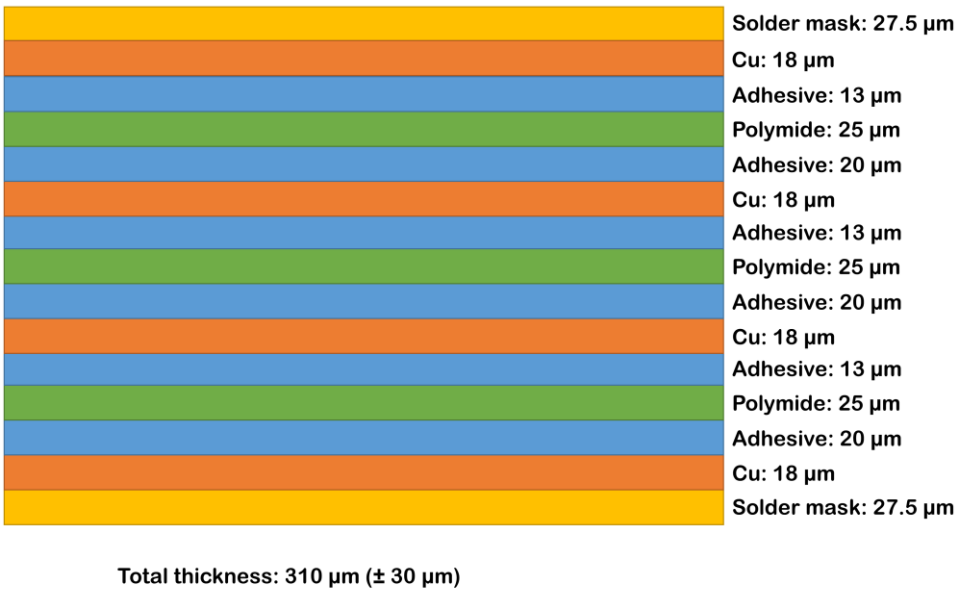

Figure 3.3. Flexible printed circuit stack-up for sensor platform.

The battery voltage is regulated by a boost-converter (TPS61220DCK, Texas Instruments Inc.), also the smallest available of its kind. Both boost converter and battery are decoupled by two capacitors each. The standard regulated voltage is 3.0 V, but can be adjusted between 2.7 V and 5.25 V by changing

the ratio of a resistor pair in the feedback loop. A ferrite bead protects the circuit from environmentally induced noise.

The main controlling unit is a combined microcontroller and Bluetooth Low Energy (BLE) controller, the CC2540 system-on-chip (Texas Instruments Inc.). The microcontroller is based on Texas Instrument's ultra-low power architecture MSP430. The built-in BLE controller excludes the need for an additional, dedicated IC. The application utilizes the built-in 12-bit analog-to-digital converter to further limit additional components.

The amperometric and voltammetric analog front-end is the LMP91000 [85]. It is currently the only commercially available chip potentiostat, and has been for many years [86], [87]. It is based on a conventional two-opamp design: A control amplifier to maintain the cell potential, as in Figure 2.3, and a transimpedance amplifier for reading out the current as a voltage. The cell potential can be programmatically configured to 27 discrete levels. The amplification of the current is configured to seven different levels by internal gain resistors, with the eighth choice of setting an external resistor. A capacitor can be added to the feedback loop for active low-pass filtering. This was not used in any of the reported applications due to rapid potential changes, but will be more useful for fixed-potential applications, and hence made room for in the layout. With a 3V regulated power supply the voltammetric capabilities span bias voltages of ± 720 mV, currents up to ± 873 µA with a minimum resolution of 0.86 nA.

The second front-end is an instrumentation amplifier, the MAX4461, and is meant exclusively for open-circuit potentiometry. OCP is particularly important for ion-selective electrodes, such as pH, K^+ and Na^+ sensors. It is the smallest commercially available fixed-gain instrumentation amplifier. It is quite limited in terms of dynamic range, with a linear response in the range 10-300-mV. Although limited, it can still accommodate a range of potentiometric sensors, since their sensitivities rarely surpass the 59 mV per decade dictated by the Nernst equation, and the span can be shifted to the compatible range by selecting an appropriate reference electrode. When the sensor platform is set to utilize the MAX4461 as the front-end, the ADC reference voltage is

changed to the internal band-gap reference volt age (1.27 V) rather than the supply voltage, to better utilize the dynamic range. The resulting voltage resolution is 310 µV.

The BLE transmission line consists of an impedance matching balun and a chip antenna. The leads connecting the two were made symmetrical and equal in length to limit impedance mismatch. The lead connecting the balun and chip antenna was designed with a characteristic impedance of 50 Ω by adjusting its width, according to Wheeler's microstrip line equation [88], to 127 µm, given copper track thickness and dielectric height as defined by the stack-up in Figure 3.3, and a dielectric constant of polyimide of 3.2. It was able to transmit with a signal strength up to 45 dBm and maintained the connection up to at least 15 m in line-of-sight.

The transducer (sensor head) is isolated to its own peninsula protruding from the main body of the circuit to protect the electronic components from the test solution. It is situated close to the analog front-ends (15 mm) in order to minimize the analog signal path, and thus the environmentally induced noise. Connection to the electrodes is done via small (Ø300 µm), Au-plated contact pads. The electrodes are defined by the screen-printing masks or stencils, and lends some freedom to design the electrodes to the specific application. The electrode design is constricted by the outline of the peninsula and the fact they have to make electrical contact with the contact pads. E.g. a two-electrode setup can be achieved by one electrode shorting the reference and counter electrode, or their geometrical shape may be changed. In this work we have exclusively used relatively large, parallel band electrodes (4 mm × 1.25 mm with rounded edges) pitched 1.80 mm apart. This was done to remain safely within the technical limitations of screen-printing, and thus maximizing the reproducibility of surface area-dependent signals.

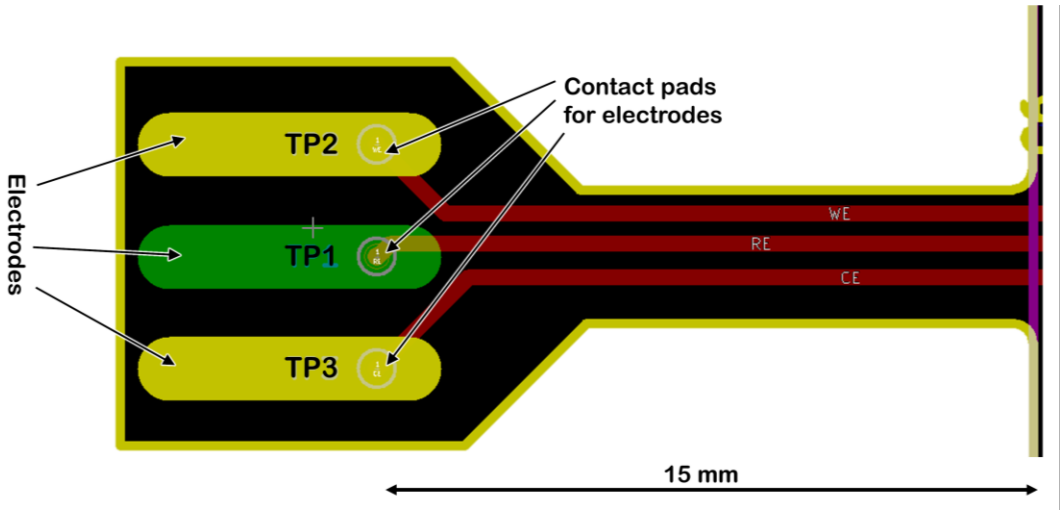

Figure 3.4. Parallel band electrodes (TP1-3). From the top, working (TP2), reference (TP1) and counter electrode (TP3).

Opposite the electrodes, a second, larger peninsula holds functionality for programming and debugging the circuit. The signal lines connect via a custom-made, 3D-printed, dual row edge connector (2.54 mm pitch), but might also be soldered directly to the gold-plated contact pads. The individual electrodes are made addressable through this bus. This allows both bypassing the on-board circuitry, and connection o the electrodes to external instrumentation, as well as interfacing a external electrodes with the circuit. This way, both sensor and instrumentation can be verified in isolation. The debugging part of the circuit is designed such that it may be cut off to further reduce size and weight. Once cut-off, the circuit cannot be reprogrammed. The hardware design files are available online (https://github.com/sindresops/ecFlex-HW).

3.1.2 Firmware

The firmware is based around the software example “SensorBLEPeripheral” bundled with the application note TIDA-00056 [89]. Among the major modifications of the code is the added support for the MAX4461, and the measurement modes OCP, SWV, CCSWV, SWA, biased CA , MA. The handling of the temperature readout was altered to return the internal temperature of the microcontroller if the voltammetry front-end’s temperature sensor was offline, e.g. in OCP mode. An SPI communications protocol was added as an option, in case the user would wish to connect the device to a master unit,

such as a smart watch or wristband. All configurable parameters, such as voltammetry, and potentiometry settings and sample frequency was collected in separate hardware files, one unique per technique. The source code is available online (https://github.com/sindresops/ecFlex-FW).

3.1.3 Software

Texas Instruments provides the iPhone (Apple Ïnc.) application “TI gas sensor” for reading out sensor data from chipsets utilizing the CC25xx-range of microcontrollers. It is however limited to a maximum number of datapoints, meaning the oldest datapoints are discarded from the savable data buffer. It also does not log temperature, only displays it. Since the source code contains syntax no longer supported by Apple Inc,. the code could not be modified to improve upon these shortcomings. An application code for Windows (Microsoft) was developed to resolve these shortcomings.

The code was written in C# using Visual Studio 2017 (v. 15.8.2) with the GATT (generic attribute) protocol BLE protocol, and the according libraries. The main window is depicted in Figure 3.5. The software picks up any BLE device broadcasting with the SSID (service set identifier) “ecFlex”. Upon successful connection, the technique specific parameters are read from specific GATT addresses, or handles. The computer then subscribes to the handle containing the sensor data, and outputs said data on a live graph, and an indicator panel. The sensor data may be saved to a comma separated file at any time during or after the measurement. The data is also autosaved for each new datapoint. The software is programmed to re-establish the connection if lost or timed out. This allows the connection to be sustained if the sensor temporarily moves out of range, or the transmission medium changes. The executable and source code is available online (https://github.com/sindresops/ecFlex-SW).

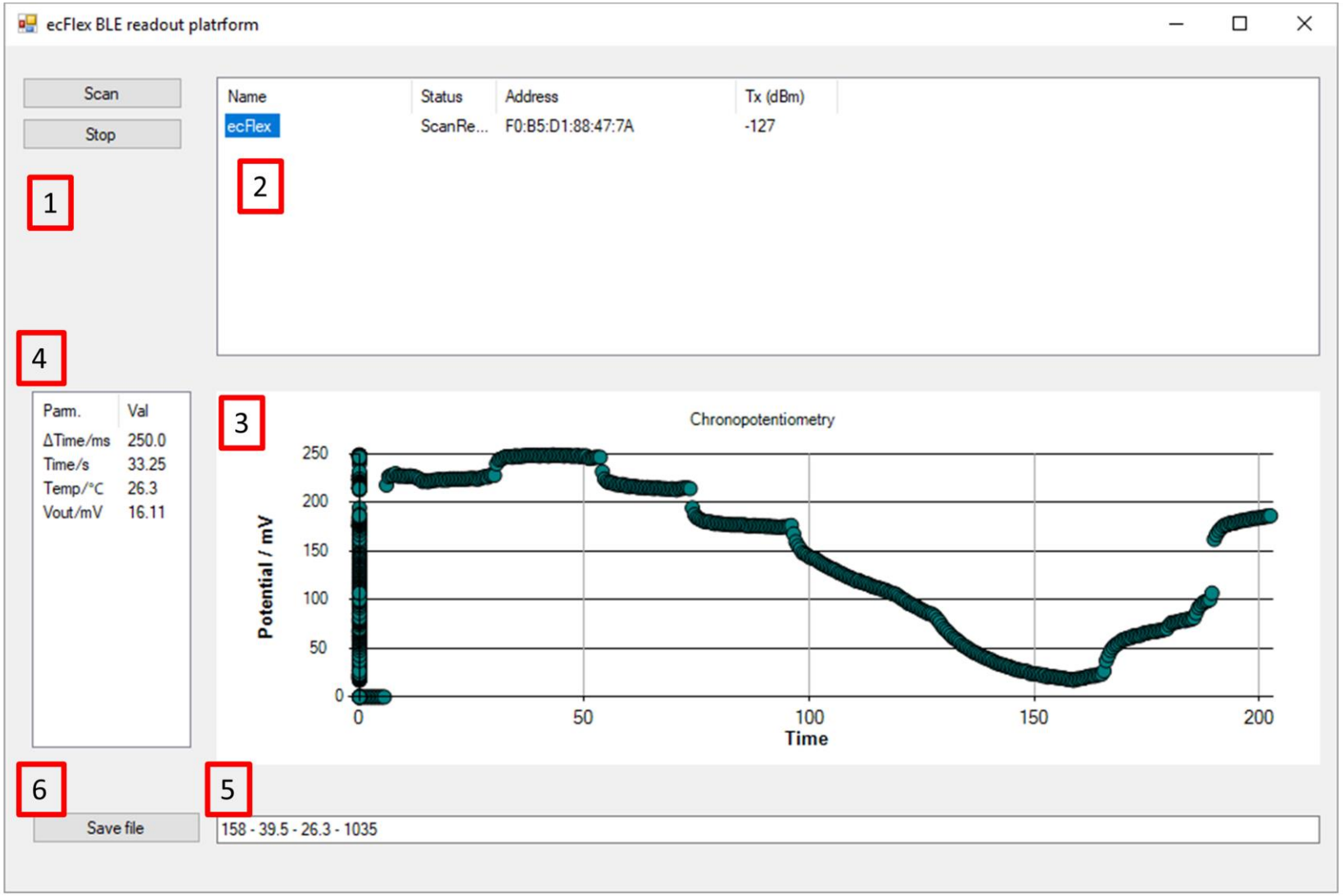

Figure 3.1. Bluetooth readout software for electrochemical sensor platform. The main components are (1) start and stop search for BLE broadcasting ecFlexes, (2) list of broadcasting devices, (3) live plot area, (4) indicator panel showing sampling frequency, time since measurement start, on-board temperature and instantaneous signal, (5) status window for displaying status messages and (6) button prompting a file dialog for saving the raw data.

3.1.4 Platform specifications

The sensor platform is compared to other open-source potentiostats in Table 3.II. It distinguishes itself by being (i) mechanically flexible, (ii) light, (iii) small, (iv) having integrated electrodes, providing (v) portability by being battery operated and wireless, while (vi) incorporating a range of different measurement techniques, being the (vi) second cheapest in the collection. In return it suffers from (i) limited voltammetric and (ii) potentiometric range, compared to the other instruments. Even though that does not notably affect the sensor schemes demonstrated in Articles II and III, it does impede on the universality of the sensor platform. A potential user is more likely do be limited by the precision and range of the instrument compared to the other open-source potentiostats. However, if the assay can be designed to fit within these limitations, the user already possesses a product it for demonstration, having circumvented the development of an application specific device.

Table 3.I. Properties of open-source potentiostat compared.

	UWED [83]	**CheapStat** [81]	**PSoC-Stat** [78]	**DSTAT** [79]	**Rodeostat**	**ecFlex (this work)**
Special features			Single chip configurable design		Web GUI	Temperature Flexible Integrated electrodes
Physical dimensions	~30 × 50 × 10 mm (estimate)	140 × 66 × 28 mm	~70 × 20 × 1.5 mm (estimate)	92 × 84 × 31 mm	N/A	25 × 29 × 0.8 mm
Weight	N/A	N/A	N/A	N/A	N/A	1.2g
Connectivity PC	BLE	USB	USB	USB	USB	BLE, SPI
Connectivity cell phones	BLE	N/A	N/A	N/A	N/A	BLE
Techniques	CA, OCP, CV, SWV, DPV	CA, CV, SWV	CA, CV	CA, OCP, CV, SWV, DPV	CA, MA, OCP, CV	CA, SWA, SWV, MA, OCP, CSCV, CCSW,
Voltammetric range/resolution	±180 µA / 6.4 nA ±1.5 V / 67 µV	±50 µA ±1.0 V / 1 mV	±2.0 V / 1 mV	0-3V / 46 µV	± 1000 µA / N/A ±10 V / N/A	± 872 nA / 0.87 nA ± 720 mV / 60 mV
Potentiometric range/resolution	Not specified	N/A	N/A	Not specified		10-300 mV / 310 µV
Material cost	$61	$80	$10	$120	$250	€25
Power source	Rechargeable battery	2 × AA batteries, USB	USB	USB		Flexible battery or USB
Hardware interface	Smartphone/tablet app	LCD, PC GUI	PC GUI		Web interface	iPhone app or PC app

4 Summary of contributions

4.1 Paper I - Long-Term Potential Stability of Screen-Printed Pseudo-Reference Electrodes for Electrochemical Biosensors

In this in-depth study, screen-printed pseudo-reference electrodes of different material compositions are investigated for their electrochemical potential stability over an extended period of time. An automated experimental setup was designed such that the OCP of up to 11 reference electrodes could be probed simultaneously while only requiring one precision voltmeter. The image in Figure 4.1 depicts the setup. A PCB provides electrical connections between a center reference electrode and the 11 surrounding test electrodes. It also provides mechanical support and serves as a lid that covers the beaker containing the test solution. Mechanical relays controls which test electrode is being measured vs. the central reference electrode. Connections were made to the external instrument via a through-hole mounted header. The graphic was not included in the final publication, and is hence printed here. A generic protocol was developed to assess the electrodes' suitability in long-term applications. The electrode systems studied were Ag, 3:1 Ag/AgCl, 9:1 Ag/AgCl, Ag/Pd and Pt. Their potentials were continuously probed in phosphate buffered saline solution over the course of 40 days, and characterized by energy dispersive x-ray spectroscopy, scanning electron microscopy and cyclic voltammetry before and after this period. The electrode stability was determined by their OCPs relative to the initial electrode potential recorded when the experiment commenced on day one ($t(\,|E\,-\,E(t=0)|\,<\,30\,mV\,)$). Pt proved the least stable with a lifetime spanning less than a day, whereas 3:1 Ag/AgCl was the only material system which lifetime exceeded the 40 days. The 9:1 Ag/AgCl electrodes did not have sufficient Ag/AgCl to maintain a stable potential for more than 38 days due to complete dissolution, as confirmed by EDX. Ag shared the Cl^- affinity of Ag/AgCl, but was more prone to mixed potential contributions, and thus did not fulfil the stability

requirement for more than two days. Ag/AgPd lasted marginally longer (3.5 days), but exhibited erratic potential variations that could impede on biosensor performance.

Candidate's contribution: Original idea, design of experimental setup, all experimental work, simulation, and main author.

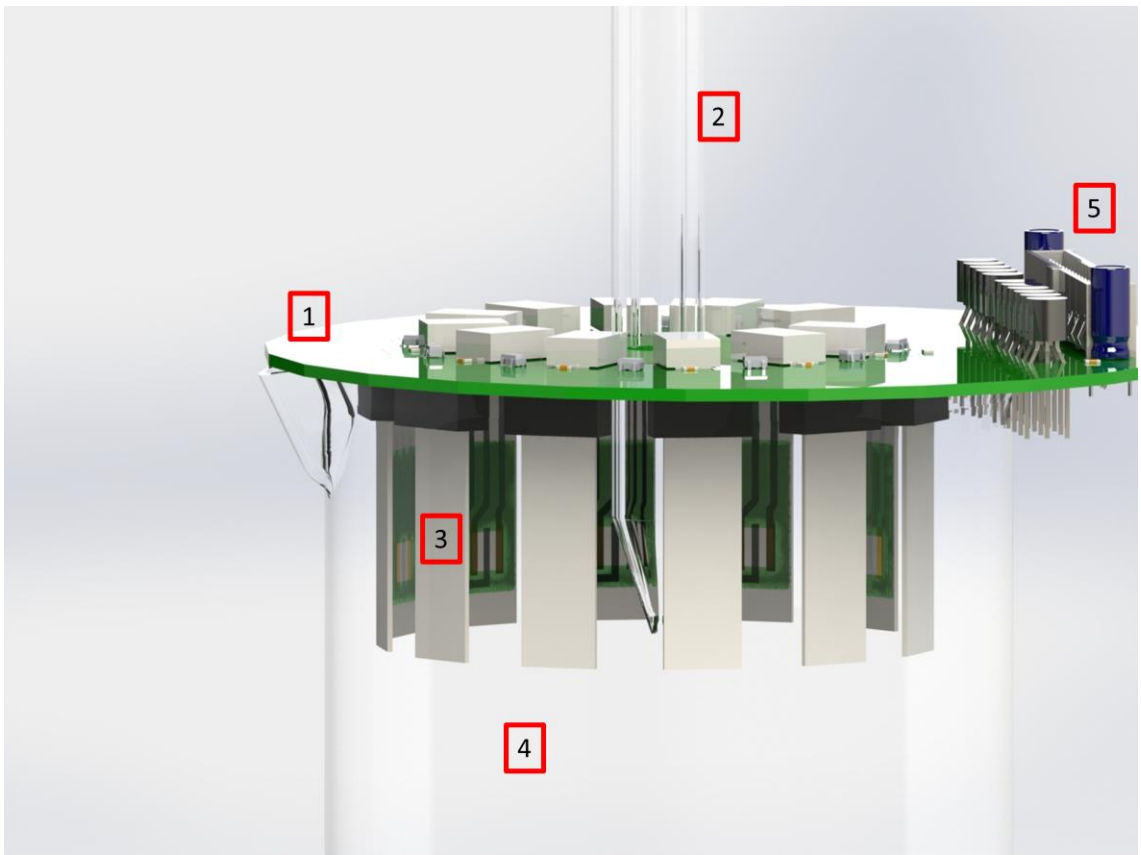

Figure 4.1. Graphical representation of setup for long-term potential monitoring of electrochemical sensors. The numbers indicate the (1) PCB, (2) central reference electrode, (3) surrounding test electrodes, (4) beaker containing test solution and (5) connector to external instrumentation.

4.2 Paper II - Hybrid electrochemical sensor platform for capsaicin determination using coarsely stepped cyclic squarewave voltammetry

The electrochemical sensor platform is presented for the first time. It was showcased by the application of detecting capsaicinoid content, the group of chemicals responsible for the pungency of chilies. This was done through adsorptive stripping voltammetry, a process that when originally proposed, was destructive and designed for disposable electrodes. It was made compatible with the sensor platform by adapting the instrumental mode from cyclic voltammetry to coarsely-stepped cyclic squarewave voltammetry, and by the development of an electrode cleaning protocol that allowed for reusing the sensor. In contrast to previous reports, by leaving the graphite working electrode unmodified, it was able to analyze a broader analytical range (up to 5000 µM, LOD = 1.98 µM). The assay transferred to the sensor platform exhibited performance characteristic comparable to those using more refined techniques, e.g. cyclic voltammetry, as well as those modified with carbon nanotubes, despite employing no electrode modification.

Candidate's contribution: Original idea, all experimental work, circuit design, protocol design, application specific firmware programming, and main author.

4.3 Paper III - Chloride and pH Determination on a Wireless, Flexible Electrochemical Sensor Platform

The versatility of the sensor platform is increased by introducing two new sensor architectures and two new instrumental modes. OCP was used for pH sensing, and squarewave amperometry for Cl^- sensing. The pH sensor was realized by adding the pH sensitive, but little used, material graphene oxide on top of a graphite electrode containing the redox compound $Fe[CN]_6^{3-/4-}$, in order to maintain a strong equilibrium potential even at low H^+ concentration. A steady state reference electrode based on a NaCl loaded polyvinyl butyral membrane was made for the pH sensor to function independently of Cl^- content. The sensor platform was able to determine pH in the range pH 10 to pH 2 (± 0.43). with a sensitivity of 26 mV pH^{-1}. The Cl^- sensor was made using identical Ag/AgCl working and reference electrodes utilizing the technique of squarewave amperometry. The reference electrode ensured that the Ag/AgCl equilibrium was always interrogated by the working electrode perturbations due to it following the Cl^- content. The sensor principle was validated both by simulation and on the sensor platform itself. The resulting sensor was able to detect Cl^- concentration in the range pCl 3 to pCl 0 (± 0.27).

Candidate's contribution: Original ideas, all experimental work, simulations, design, experimental setups, application specific firmware programming, programming of readout software, and main author.

4.4 Paper IV - Analytical errors in biosensors employing combined counter/reference electrodes

This work further investigates the role and importance of the reference electrode in an electrochemical sensor. The hypothesis that the shift of reference potential due to polarization of the reference electrode can significantly impact the performance of a biosensor is tested. Finite element analysis is used to emulate a biosensor that uses a combined reference and counter electrode in conjunction with working electrode of

equal size. It is shown that if the operational potential of the sensor is close to that of the equilibrium of the electrode reaction, a shift in potential induced by the reference electrode may lead to lowered sensitivity due to increased contribution from the opposite oxidation state of the reactant, as well as reduced electrode kinetics. The simulated response was found to deviate up to 14 % compared to the ideal analytical signal of the biosensor. The concept is demonstrated experimentally on screen-printed electrodes.

Candidate's contribution: Original idea, simulations, experiments, and main author.

4.5 Other contributions

The candidate has made additional contributions to the field, not directly linked to the content of this thesis, through international collaborations during the project period.

Bioinspired detection sensor based on functional nanostructures of S-proteins to target the folate receptors in breast cancer cells (https://doi.org/10.1016/j.snb.2018.04.037)

Candidate's contribution: Contributed to discussion part of the mechanism behind unexpected electrochemical sensor response.

Impedance-based sensor for potassium ions (https://doi.org/10.1016/j.aca.2018.06.044).

Candidate's contribution: Revised first draft, contributed to the data analysis of impedimetric response, and contributed to the discussion on sensor response.

Sensitivity Comparison of Macro- and Micro-electrochemical Biosensors for Human Chorionic Gonadotropin (hCG) Biomarker Detection (doi: 10.1109/ACCESS.2019.2928132)

Candidate's contribution: Contributed to analysis of cyclic voltammetry data and the discussion on cyclic voltammetry.

5 Conclusion and outlook

5.1 Conclusion

This work details the development of a universal, small, portable, low-cost and mechanically flexible sensor platform for electrochemical biosensing. The resulting device is based upon a flexible printed circuit platform that measures 25 mm × 29 mm and weighs 1.2 g, with a material cost of €25. Universality was demonstrated through several electrochemical measurement techniques and quantification of three different analytes: Capsaicin through coarsely-stepped squarewave voltammetry, pH by means of open circuit potentiometry and Cl^- using squarewave amperometry. Portability was secured by wireless data transmission through Bluetooth Low Energy and 14h continuous operation by a 25 mAh battery. Screen-printed electrodes was integrated to be part of the sensor platform to eliminate potential interface between platform and external electrodes. Yet, the option to interface external electrodes for disposable applications was enabled by making the electrodes addressable via contact pads. The integrated temperature sensor enables the possibility for real-time temperature calibration.

The performance of a key component, the reference electrode, was studied in detail. In particular, the electrochemical potential stability in physiological buffer system over a 40 day period was studied for different screen-printed material systems. Out of the five systems Pt, Ag/AgPd, Ag, 9:1 Ag/AgCl and 3:1 Ag/AgCl, the latter was the only one to remain within 30 mV of its initial potential after 40 days. This was attributed to the high AgCl loading prohibiting complete dissolution in during the measurement period.

The reference electrode was further studied in a two-electrode setup to gauge the impact of electrode polarization on the sensor response. This was done trough simulation of an enzymatic biosensor where working and reference electrodes were of equal size. The sensor response was shown to markedly change as a function of the

reference electrode polarization, as much as 20 % at higher analyte concentrations. The principle was demonstrated by experiment.

The determination of chili pungency, i.e. capsaicinoid content, was demonstrated on the sensor platform. Whereas the original report uses cyclic voltammetry and disposable electrodes, the sensor platform was able to perform the assay using a less precise technique, coarsely-stepped squarewave voltammetry and reusable, integrated electrodes. The capsaicin could be detected up to 5000 µM with a lower limit of detection of 1.98 µM.

Potentiometric capability was demonstrated by the quantification of pH in the range 2 to 10 (± 0.43). This was done by modifying carbon electrodes with the pH sensitive metalloid oxide graphene oxide. In addition, the reference electrodes was modified with a solid-state polymer electrolyte doped with NaCl in order to maintain constant Cl^- level or the underlying Ag/AgCl electrode.

Finally a rarely employed technique for ion determination, squarewave amperometry, was employed for the quantification of Cl^- in the range pCl 3 to 0 (± 0.27). This method requires no electrode modification beyond that of printing the actual Ag/AgCl working, counter and reference electrodes. The technique utilizes that the Ag/AgCl reference will change with the Cl^- content, and the fast kinetics of the Ag/AgCl reaction with Cl^- to perturb the equilibrium by a small squarewave voltage (60 mVpp) waveform. The magnitude of the resulting alternating current waveform is indicative of the Cl^- concentration.

5.2 Future prospects

A natural continuation upon this work is to further expand the portfolio of sensors and techniques validated on this platform. Indeed, this is being done by commercial players that have chosen to utilize this platform for their applications. Some of the sensors are enzymatic amperometric glucose and lactate sensors for wearable applications, antibody-based cancer marker detection through coarsely-stepped cyclic voltammetry,

potentiometric potassium and sodium detection based on ionphoretic ion-sensitive electrode modifications.

A second path to follow is to improve the instrumental performance of the platform. Most imminent is improving the voltammetric range and resolution such that the platform can be used for cyclic voltammetry, a much valued technique by the community. Most of the performance of the voltammetric and amperometric techniques is limited by the chip-potentiostat, for which there are currently no other commercial contenders. Its design allows for some flexibility in that it permits an optional, external reference voltage, as an alternative to using the supply voltage. One of the improvements suggested in Article III is to connect the band-gap reference potential (~1270 mV) of the microcontroller. That would make lower potentials available to the chip potentiostat without the need of added circuitry to generate the external voltage.

Secondly, improving the potentiometric range and resolution would open the platform to a higher range of potentiometric sensing. The open circuit potentiometric mode is currently limited to a range of 10-300 mV. A tunable range could be achieved by replacing the MAX4461 with the MAX4462, which allows for negative voltage swings by having its reference terminal tied to a potential between the voltage rails in the same package size. This comes at the cost of the shutdown functionality of the MAX4461, which allows it to be set in a low-power mode when it is not in use.

The option for real-time temperature calibration of the sensor signal was not addressed in this scope. It is, however, a highly relevant topic. All chemistry is accelerated with temperature and will consequently alter the sensor response. Since the temperature for each datapoint is readily accessibly by the sensor platform, this could be a managble exercise.

Getting more out of the battery life is always a justified activity. The scope of the thesis did not permit optimization for power consumption, which means there is plenty of room for improvement. The sensor currently transmits each gathered sample, which

means the transmission part of the circuitry has to be active for most of the operational time. Collection more data and transmitting larger packets would lower power consumption. Secondary features, like temperature, can be disabled to further maximize battery life.

Although there are many desirable optimizations to be done for the current platform, its present state fulfils the overall goal and underlying sub-goals having been demonstrated as a (i) universal electrochemical instrument that can be functionalized to (ii) detect different analytes through (iii) different measurement techniques, in a (iv) format that is portable, and has (v) potential for mass-production. It is our hope that making the hardware, firmware and software open will lower the barrier for developing important sensing schemes that can help solve real-world problems.

References

[1] D. V Gibson and W. Smilor, “Key variables in technology transfer : A field-study based empirical analysis,” vol. 8, 1991.

[2] A. Günsel, “Research on Effectiveness of Technology Transfer from a Knowledge Based Perspective,” *Procedia - Soc. Behav. Sci.*, vol. 207, pp. 777–785, 2015.

[3] G. Slaughter and T. Kulkarni, “Highly Selective and Sensitive Self- Powered Glucose Sensor Based on Capacitor Circuit,” *Sci. Rep.*, no. February, pp. 1–9, 2017.

[4] M. Mazhar Rathore, A. Ahmad, and A. Paul, “IoT-based smart city development using big data analytical approach,” *2016 IEEE Int. Conf. Autom. ICA-ACCA 2016*, pp. 1–8, 2016.

[5] S. L. Bonting, *Chemical sensors for space applications*, vol. 2. Elsevier, 1992.

[6] S. Neethirajan, “Recent advances in wearable sensors for animal health management,” *Sens. Bio-Sensing Res.*, vol. 12, pp. 15–29, 2017.

[7] D. Olczuk and R. Priefer, “A history of continuous glucose monitors (CGMs) in self-monitoring of diabetes mellitus,” *Diabetes Metab. Syndr. Clin. Res. Rev.*, vol. 12, no. 2, pp. 181–187, 2018.

[8] S. Vashist, “Continuous Glucose Monitoring Systems: A Review,” *Diagnostics*, vol. 3, no. 4, pp. 385–412, 2013.

[9] C. Mathas, “Sensor Advances for Military Environments,” 2013.

[10] W. Gao *et al.*, “Fully integrated wearable sensor arrays for multiplexed in situ perspiration analysis,” *Nature*, vol. 529, no. 7587, pp. 509–514, 2016.

[11] B. S. Basu A.K., Tatiya S., Bhatt G., “Fabrication Processes for Sensors for Automotive Applications: A Review.,” in *Sensors for Automotive and Aerospace Applications. Energy, Environment, and Sustainability.*, S. S. Bhattacharya S., Agarwal A., Prakash O., Ed. Singapore: Springer, 2019.

[12] J. D. Turner and L. Austin, “A review of current sensor technologies and applications within automotive and traffic control systems,” *Proc. Inst. Mech. Eng. Part D J. Automob. Eng.*, vol. 214, no. 6, pp. 589–614, 2000.

[13] G. S. Duffó, S. B. Farina, and C. M. Giordano, “Characterization of solid embeddable reference electrodes for corrosion monitoring in reinforced concrete structures,” *Mater. Corros.*, vol. 61, no. 6, pp. 480–489, 2010.

[14] M. Jin *et al.*, “Electrochemical Characterization of Solid Ag/AgCl Reference Electrode with Different Electrolytes for Corrosion Monitoring of Steel in Concrete,” *Electrochem. Soc. Japan*, vol. 2, pp. 383–389, 2016.

[15] R. Du, R. Hu, R. Huang, and C. Lin, “In Situ Measurement of Cl - Concentrations and pH at the Reinforcing Steel / Concrete Interface by Combination Sensors,” vol. 78, no. 9, pp. 3179–3185, 2006.

[16] U. Angst, B. Elsener, C. K. Larsen, and Ø. Vennesland, “Critical chloride content in reinforced concrete - A review,” *Cem. Concr. Res.*, vol. 39, no. 12, pp. 1122–1138, 2009.

[17] J. Wang, “Electrochemical Sensors for Environmental Monitoring : A Review of Recent Technology,” pp. 1–17, 2011.

[18] F. W. Scheller, U. Wollenberger, A. Warsinke, and F. Lisdat, “Research and

development in biosensors," pp. 35–40, 2001.
[19] F. W. Scheller *et al.*, "Second generation biosensors," vol. 6, pp. 245–253, 1991.
[20] A. P. F. Turner, "Biosensors: sense and sensibility," *Chem. Soc. Rev.*, vol. 42, no. 8, p. 3184, 2013.
[21] S. Sharing, "' Publish or Perish '*," vol. 467, no. September 2010, p. 2012, 1996.
[22] U. S. Neill, "Publish or perish , but at what cost ?," vol. 118, no. 7, p. 36371, 2008.
[23] GlobalData, "Insulin Pumps - Medical Devices Pipeline Assessment, 2018," 2018. [Online]. Available: https://www.globaldata.com/store/report/gdme0542epd--insulin-pumps-medical-devices-pipeline-assessment-2018/. [Accessed: 06-Dec-2018].
[24] GlobalData, "Continuous Glucose Monitoring Systems - Medical Devices Pipeline Assessment, 2018," 2018. [Online]. Available: https://www.globaldata.com/store/report/gdme0544epd--continuous-glucose-monitoring-systems-medical-devices-pipeline-assessment-2018/. [Accessed: 06-Dec-2018].
[25] J. P. Metters, R. O. Kadara, and C. E. Banks, "New directions in screen printed electroanalytical sensors: An overview of recent developments," *Analyst*, vol. 136, no. 6, pp. 1067–1076, 2011.
[26] A. Hobby, "Screen-printing for the industrial user," 1997. .
[27] P. Rosa, A. Câmara, and C. Gouveia, "The Potential of Printed Electronics and Personal Fabrication in Driving the Internet of Things," *Open J. Internet Things*, vol. 1, no. 1, 2015.
[28] Z. Taleat, A. Khoshroo, and M. Mazloum-Ardakani, "Screen-printed electrodes for biosensing: A review (2008-2013)," *Microchim. Acta*, vol. 181, no. 9–10, pp. 865–891, 2014.
[29] E. Crouch, D. C. Cowell, S. Hoskins, R. W. Pittson, and J. P. Hart, "A novel, disposable, screen-printed amperometric biosensor for glucose in serum fabricated using a water-based carbon ink," *Biosens. Bioelectron.*, vol. 21, no. 5, pp. 712–718, 2005.
[30] K. Malzahn, J. R. Windmiller, G. Valdés-Ramírez, M. J. Schöning, and J. Wang, "Wearable electrochemical sensors for in situ analysis in marine environments," *Analyst*, vol. 136, no. 14, p. 2912, 2011.
[31] A. Kagie *et al.*, "Flexible rolled thick-film miniaturized flow-cell for minimally invasive amperometric sensing," *Electroanalysis*, vol. 20, no. 14, pp. 1610–1614, 2008.
[32] G. Hughes, R. M. Pemberton, P. Nicholas, and J. P. Hart, "Fabrication of Miniaturised Screen-Printed Glucose Biosensors , using a Water-Based Ink , and the Evaluation of their Electrochemical Behaviour," pp. 1–6, 2018.
[33] C. W. Foster, J. P. Metters, and C. E. Banks, "Ultra flexible paper based electrochemical sensors: Effect of mechanical contortion upon electrochemical performance," *Electroanalysis*, vol. 25, no. 10, pp. 2275–2282, 2013.
[34] A. René, C. Cugnet, D. Hauchard, and L. Authier, "Use of screen-printed microelectrodes working as generator/collector systems for the determination of the antioxidant capacity of phenolic compounds," *Analyst*, vol. 138, no. 7, pp.

2192–2198, 2013.
[35] F. Tan, J. P. Metters, and C. E. Banks, “Electroanalytical applications of screen printed microelectrode arrays,” *Sensors Actuators, B Chem.*, vol. 181, pp. 454–462, 2013.
[36] J. O. M. Bockris, A. K. N. Reddy, and M. E. Gamboa-Aldeco, *Modern Electrochemistry 2A: Fundamentals of Electrodics*. Springer US, 2001.
[37] P. N. Bartlett, *Bioelectrochemistry: Fundamentals, Experimental Techniques and Applications*. Wiley, 2008.
[38] G. Gritzner, G. Inzelt, A. Lewenstam, and F. Scholz, *Handbook of Reference Electrodes*. Springer Berlin Heidelberg, 2013.
[39] E. C. Rama, “Bioelectroanalysis in a Drop : Construction of a Glucose Biosensor,” 2017.
[40] J. Biscay, E. C. Rama, M. B. G. García, J. M. P. Carrazón, and A. C. García, “Enzymatic sensor using mediator-screen-printed carbon electrodes,” *Electroanalysis*, vol. 23, no. 1, pp. 209–214, 2011.
[41] A. J. Bard and L. R. Faulkner, *Electrochemical methods : fundamentals and applications*. 2001.
[42] Ł. Tymecki and R. Koncki, “Screen-printed reference electrodes for potentiometric measurements,” vol. 526, pp. 3–11, 2004.
[43] U. Guth, F. Gerlach, M. Decker, W. Oelßner, and W. Vonau, “Solid-state reference electrodes for potentiometric sensors,” *J. Solid State Electrochem.*, vol. 13, no. 1, pp. 27–39, 2009.
[44] M. Hashimoto, S. Upadhyay, S. Kojima, H. Suzuki, K. Hayashi, and K. Sunagawa, “Needle-Type Ag/AgI Reference Electrode with a Stagnant Electrolyte Layer and an Active Liquid Junction,” *J. Electrochem. Soc.*, vol. 153, no. 7, p. H155, 2006.
[45] I. Shitanda, H. Kiryu, and M. Itagaki, “Improvement in the long-term stability of screen-printed planar type solid-state Ag/AgCl reference electrode by introducing poly(dimethylsiloxane) liquid junction,” *Electrochim. Acta*, vol. 58, no. 1, pp. 528–531, 2011.
[46] I. Shitanda, M. Komoda, Y. Hoshi, and M. Itagaki, “An instantly usable paper-based screen-printed solid-state KCl/Ag/AgCl reference electrode with long-term stability,” *Analyst*, vol. 140, no. 19, pp. 6481–6484, 2015.
[47] A. Cranny *et al.*, “Lifetime performance characteristics of screen-printed potentiometric Ag/AgCl chloride sensors,” pp. 2–3, 2010.
[48] N. Harris, A. Cranny, M. Rivers, K. Smettem, and E. G. Barrett-Lennard, “Application of Distributed Wireless Chloride Sensors to Environmental Monitoring: Initial Results,” *IEEE Trans. Instrum. Meas.*, vol. 65, no. 4, pp. 736–743, 2016.
[49] H. Suzuki and H. Shiroishi, “Microfabricated Liquid Junction Ag / AgCl Reference Electrode and Its Application to a One-Chip Potentiometric Sensor,” *Structure*, vol. 71, no. 22, pp. 5069–5075, 1999.
[50] N.-H. Kwon, K.-S. Lee, M.-S. Won, and Y.-B. Shim, “An all-solid-state reference electrode based on the layer-by-layer polymer coating,” *Analyst*, vol. 132, no. 9, p. 906, 2007.

[51] F. J. Andrade, T. Guinovart, G. A. Crespo, F. X. Rius, and F. J. Andrade, “A reference electrode based on polyvinyl butyral (PVB) polymer for decentralized chemical measurements,” *Anal. Chim. Acta*, vol. 821, pp. 72–80, Apr. 2014.

[52] M. Sophocleous and J. K. Atkinson, “A review of screen-printed silver/silver chloride (Ag/AgCl) reference electrodes potentially suitable for environmental potentiometric sensors,” *Sensors Actuators, A Phys.*, vol. 267, pp. 106–120, 2017.

[53] K. Idegami, M. Chikae, N. Nagatani, E. Tamiya, and Y. Takamura, “Fabrication and characterization of planar screen-printed Ag/AgCl reference electrode for disposable sensor strip,” *Jpn. J. Appl. Phys.*, vol. 49, no. 9 PART 1, 2010.

[54] J. R. Castle and W. K. Ward, “Amperometric glucose sensors: Sources of error and potential benefit of redundancy,” *J. Diabetes Sci. Technol.*, vol. 4, no. 1, pp. 221–225, 2010.

[55] J. Boswell, *Instrumental Methods in Electrochemistry*, no. March. 2007.

[56] N. A. Morris, M. F. Cardosi, B. J. Birch, and A. P. F. Turner, “An electrochemical capillary fill device for the analysis of glucose incorporating glucose oxidase and ruthenium (III) hexamine as mediator,” *Electroanalysis*, vol. 4, no. 1, pp. 1–9, 1992.

[57] Y. Zhang, Y. Hu, G. S. Wilson, D. Moatti-Sirat, V. Poitout, and G. Reach, “Elimination of the Acetaminophen Interference in an Implantable Glucose Sensor,” *Anal. Chem.*, vol. 66, no. 7, pp. 1183–1188, 1994.

[58] P. Trinidad and F. Walsh, “Conversion Expressions for Electrochemical Reactors which Operate under Mass Transport Controlled Reaction Conditions , Part I: Batch Reactor , PFR and CSTR,” *Int. J. Engng.*, vol. 14, no. 6, pp. 431–441, 1998.

[59] P. Trinidad, F. Walsh, and D. Gilroy, “Conversion expressions for electrochemical reactors which operate under mass transport controlled reaction conditions, part II: Batch reactor, PFR and CSTR,” *Int. J. Eng. Educ.*, vol. 14, no. 6, pp. 431–441, Jan. 1998.

[60] H. Wu, H. Ohnuki, S. Ota, M. Murata, Y. Yoshiura, and H. Endo, “New approach for monitoring fish stress: A novel enzyme-functionalized label-free immunosensor system for detecting cortisol levels in fish,” *Biosens. Bioelectron.*, 2016.

[61] R. T. Kachoosangi, G. G. Wildgoose, and R. G. Compton, “Carbon nanotube-based electrochemical sensors for quantifying the ‘heat’ of chilli peppers: the adsorptive stripping voltammetric determination of capsaicin,” *Analyst*, vol. 133, no. 7, p. 888, 2008.

[62] B. G. Cox, “Square-wave amperometry,” *J. Electroanal. Chem.*, vol. 136, no. 1, pp. 93–104, 1982.

[63] A. Hulanicki and W. Jedral, “Analytical possibilities of square-wave amperometry,” *Anal. Chim. Acta*, vol. 219, no. C, pp. 37–44, 1989.

[64] P. R. Roberge and R. Pierre, *Handbook of Corrosion Engineering Library of Congress Cataloging-in-Publication Data*. 1999.

[65] Y. Yard and Ş. Zühre, “Electrochemical evaluation and adsorptive stripping voltammetric determination of capsaicin or dihydrocapsaicin on a disposable pencil graphite electrode,” *Talanta*, vol. 112, pp. 11–19, 2013.

[66] E. P. Randviir, J. P. Metters, J. Stainton, and C. E. Banks, “Electrochemical impedance spectroscopy versus cyclic voltammetry for the electroanalytical sensing of capsaicin utilising screen printed carbon nanotube electrodes,” *Analyst*, vol. 138, no. 10, p. 2970, 2013.

[67] S. D. Senturia, “Simulation and design of microsystems : a10-year perspective,” vol. 67, 1998.

[68] S. D. Senturia, *Microsystem Design*. Springer US, 2007.

[69] G. Gerlach and A. Klein, “Strategies of modelling and simulation of microsystems with electromechanical energy conversion,” vol. 29, pp. 773–783, 1998.

[70] I. J. Cutress, E. J. F. Dickinson, and R. G. Compton, “Analysis of commercial general engineering finite element software in electrochemical simulations,” *J. Electroanal. Chem.*, vol. 638, no. 1, pp. 76–83, 2010.

[71] A. Lavacchi, U. Bardi, C. Borri, S. Caporali, a. Fossati, and I. Perissi, “Cyclic voltammetry simulation at microelectrode arrays with COMSOL Multiphysics,” *J. Appl. Electrochem.*, vol. 39, no. 11, pp. 2159–2163, 2009.

[72] T. J. Davies, C. E. Banks, and R. G. Compton, “Voltammetry at spatially heterogeneous electrodes,” *J. Solid State Electrochem.*, vol. 9, no. 12, pp. 797–808, 2005.

[73] U. Wollenberger, “Electrochemical Biosensors - Ways to Improve Sensor Performance Electrochemical Biosensors - Ways to Improve Sensor Perfonnance *,” vol. 13, no. 1, pp. 237–266, 1996.

[74] H. Y. Y. Nyein *et al.*, “A Wearable Electrochemical Platform for Noninvasive Simultaneous Monitoring of Ca2+ and pH,” *ACS Nano*, vol. 10, no. 7, pp. 7216–7224, 2016.

[75] A. Martín *et al.*, “Epidermal Microfluidic Electrochemical Detection System: Enhanced Sweat Sampling and Metabolite Detection,” *ACS Sensors*, vol. 2, no. 12, pp. 1860–1868, 2017.

[76] A. Afanasiev *et al.*, “A contact lens with integrated telecommunication circuit and sensors for wireless and continuous tear glucose monitoring,” *J. Micromechanics Microengineering*, vol. 22, no. 7, p. 075007, 2012.

[77] G. Matzeu, L. Florea, and D. Diamond, “Advances in wearable chemical sensor design for monitoring biological fluids,” *Sensors Actuators, B Chem.*, vol. 211, pp. 403–418, 2015.

[78] P. Lopin and K. V. Lopin, “PSoC-Stat: A single chip open source potentiostat based on a Programmable System on a Chip,” *PLoS One*, vol. 13, no. 7, pp. 1–21, 2018.

[79] M. D. M. Dryden and A. R. Wheeler, “DStat: A versatile, open-source potentiostat for electroanalysis and integration,” *PLoS One*, vol. 10, no. 10, pp. 1–17, 2015.

[80] A. Nemiroski *et al.*, “Universal mobile electrochemical detector designed for use in resource-limited applications,” *Proc. Natl. Acad. Sci.*, vol. 111, no. 33, pp. 11984–11989, 2014.

[81] A. A. Rowe *et al.*, “Cheapstat: An open-source, ‘do-it-yourself’ potentiostat for analytical and educational applications,” *PLoS One*, vol. 6, no. 9, 2011.

[82] “Rodeostat: open source potentiostat.” [Online]. Available: https://sites.google.com/iorodeo.com/potentiostat. [Accessed: 13-Nov-2019].

[83] A. Ainla *et al.*, “Open-Source Potentiostat for Wireless Electrochemical Detection with Smartphones,” *Anal. Chem.*, vol. 90, no. 10, pp. 6240–6246, 2018.
[84] Brightvolt, “BV-452229-17ET,” 2018.
[85] Texas Instruments, “LMP91000 Sensor AFE System : Configurable AFE Potentiostat for Low-Power Chemical Sensing Applications,” no. March. 2013.
[86] A. H. Jalal, Y. Umasankar, P. J. Gonzalez, A. Alfonso, and S. Bhansali, “Multimodal technique to eliminate humidity interference for specific detection of ethanol,” *Biosens. Bioelectron.*, vol. 87, pp. 522–530, 2017.
[87] A. F. D. Cruz, N. Norena, A. Kaushik, and S. Bhansali, “A low-cost miniaturized potentiostat for point-of-care diagnosis,” *Biosens. Bioelectron.*, vol. 62, pp. 249–254, 2014.
[88] H. A. Wheeler, “Properties of a Strip on a Sheet on a Plane,” no. 8, 1977.
[89] A. Singh, “Gas Sensor Platform Reference Design,” no. August, 2013.

Errata

In article II, σ-benzenoquone shoud be 1,2-benzoquinone.

Appendix A – Sensor platform schematic

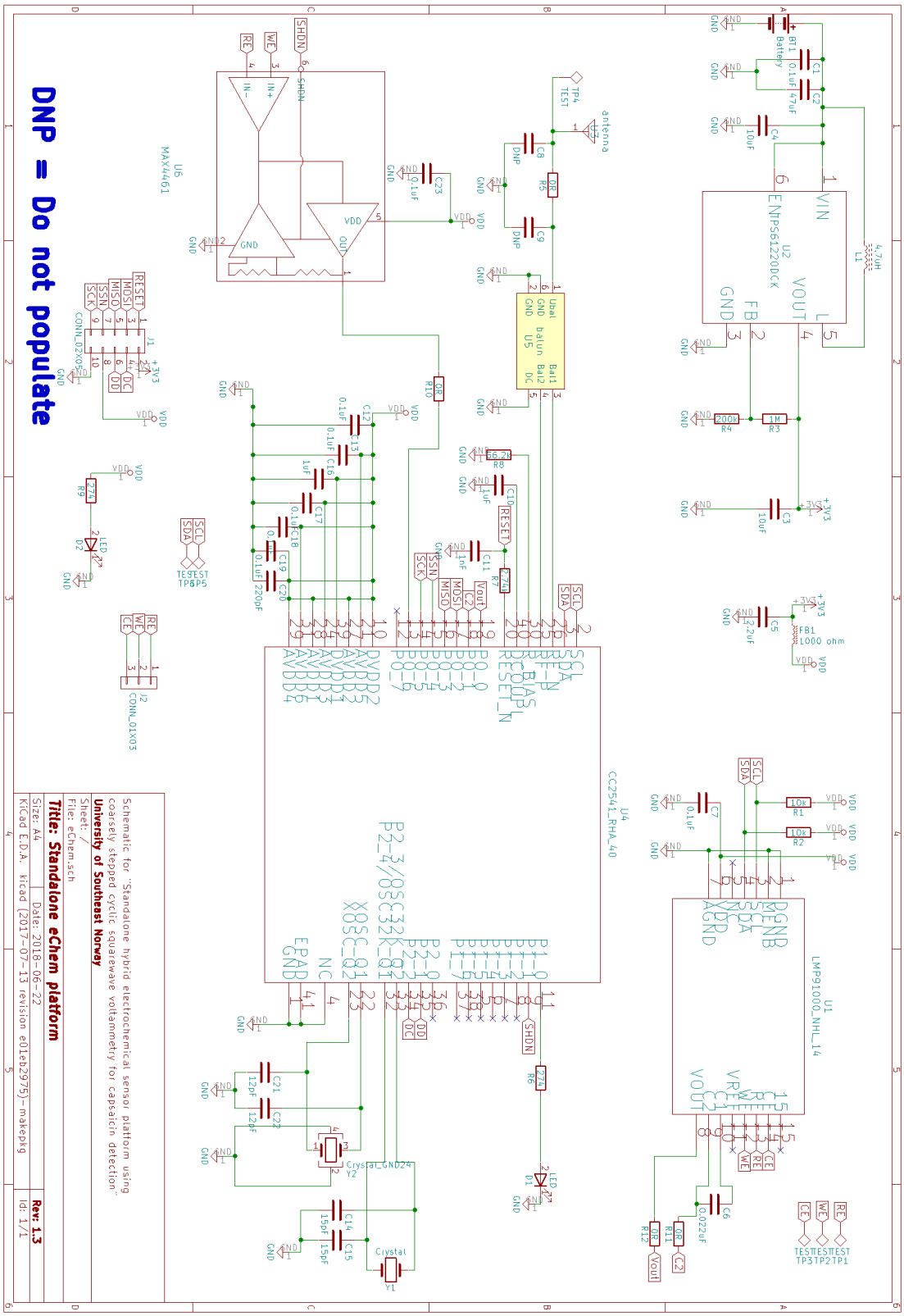

Appendix B – Sensor platform bill-of-materials

Reference	Quantity	Value	Part No.	Manufacturer	Unit (€)	Total (€)
BT1	1	Battery	BV-452229-25ST	BrightVolt	€ 2.000	€ 2.000
C1 C12 C13 C17 C18 C19 C23 C7	8	0.1uF	GRM155R71A104KA01D	MuRata	€ 0.071	€ 0.571
C10 C16	2	1uF	GRM155R61A105KE15D	MuRata	€ 0.071	€ 0.143
C11	1	1nF	GRM1555C1H102JA01D	MuRata	€ 0.071	€ 0.071
C14 C15	2	15pF	GRM1555C1H150JA01D	MuRata	€ 0.071	€ 0.143
C2	1	47uF	GRM31CR60J476KE19L	MuRata	€ 0.071	€ 0.071
C20	1	220pF	GRM1555C1H221JA01D	MuRata	€ 0.071	€ 0.071
C21 C22	2	12pF	GRM1555C1H120JA01D	MuRata	€ 0.071	€ 0.143
C3 C4	2	10uF	GRM188R60J106ME47D	MuRata	€ 0.071	€ 0.143
C5	1	2.2uF	GRM155R60J225ME15D	MuRata	€ 0.071	€ 0.071
C6	1	0.022uF	GRM155R71C223KA01D	MuRata	€ 0.071	€ 0.071
C8 C9	2	DNP	GRM155R60J225ME15D	MuRata	€ 0.071	€ 0.143
D1 D2	2	LED	SMLP12BC7TT86	Rohm	€ 0.429	€ 0.857
FB1	1	1000 ohm	BLM31KN102SH1L	MuRata	€ 0.114	€ 0.114
L1	1	4.7uH	EPL3015-472MLB	Coilcraft	€ 1.429	€ 1.429
R1 R2	2	10k	CRCW040210K0FKED	Vishay	€ 0.114	€ 0.229
R3	1	1M	CRCW04021M00JNED	Vishay	€ 0.114	€ 0.114
R4	1	200k	CRCW040220K0JNED	Vishay	€ 0.114	€ 0.114
R10 R11 R12 R5	4	0R	CRCW04020000ZSTD	Vishay	€ 0.114	€ 0.457
R6 R9	2	274	CRCW0402274RFKED	Vishay	€ 0.114	€ 0.229
R7	1	2.74k	CRCW04022R74FKTD	Vishay	€ 0.114	€ 0.114
R8	1	56.2k	CRCW040256K2FKED	Vishay	€ 0.114	€ 0.114
TP1 TP2 TP3 TP5 TP6	5	TEST			€ 0.000	€ 0.000
TP4	1	TEST			€ 0.000	€ 0.000
U1	1	LMP91000_NHL_14	LMP91000SDE	TI	€ 4.300	€ 4.300
U2	1	TPS61220DCK	TPS61220	TI	€ 1.286	€ 1.286
U3	1	antenna	2450AT18A100	Johnson Technology	€ 0.571	€ 0.571
U4	1	CC2541_RHA_40	CC2541	TI	€ 4.429	€ 4.429
U5	1	balun	2450BM15B0002	Johanson Technology	€ 1.000	€ 1.000
U6	1	MAX4461	MAX4461TEUT-T	MAXIM	€ 2.857	€ 2.857
Y1	1	Crystal	ABS07-32.768KHZ-9-T	Abracon Coroporation	€ 1.000	€ 1.000
Y2	1	Crystal_GND24	FA-128 32.0000MF20X-K3	Epson	€ 1.429	€ 1.429
Ag/AgCl ink	1	Electrode	C2130823D1	Gwent Electronics Inc.	€ 0.100	€ 0.100
Graphite ink	1	Electrode	C2000802P2	Gwent Electronics Inc.	€ 0.100	€ 0.100
Flex circuit board	1	PCB		Custom made	€ 1.000	€ 1.000
						€ 25.486

Article 1

S. Søpstad, E. A. Johannessen, F. Seland, and K. Imenes (2018). Long-term stability of screen-printed pseudo-reference electrodes for electrochemical biosensors, *Electrochim. Acta*, vol. 287, pp. 29–36. doi: 10.1016/j.electacta.2018.08.045

Article 2

S. Søpstad, K. Imenes, and E. A. Johannessen (2019). Hybrid electrochemical sensor platform for capsaicin determination using coarsely stepped cyclic squarewave voltammetry, *Biosens. Bioelectron.*, vol. 130, pp. 374–381. doi: 10.1016/j.bios.2018.09.036

Article 3

S. Søpstad, K. Imenes, and E. A. Johannessen (2019). Chloride and pH detection on flexible a electrochemical sensor platform, *IEEE Sensors Journal (Early Access),* doi: 10.1109/JSEN.2019.2944407

Article omitted from online version due to publisher's restrictions

Article 4

S. Søpstad, K. Imenes, and E. A. Johannessen (2019). Analytical errors in biosensors employing combined counter/reference electrodes. Submitted to *Results in Chemistry* July 2019

Article omitted from online version due to publisher's restrictions

Doctoral dissertation no. 54
2019
—

Flexible electrochemical sensor platform
Dissertation for the degree of PhD
—
Sindre Søpstad
—
ISBN: 978-82-7860-404-5 (print)
ISBN: 978-82-7860-405-2 (online)

usn.no